Characterization of the Role of Transferrin receptor 1 (Tfr1) in the Intestinal Epithelium, Pancreas, and Skin

by

Alan Chen

Department of Pharmacology and Cancer Biology
Duke University

Date:_______________________
Approved:

____
Nancy Andrews, Supervisor

____
David Kirsch

____
Terry Lechler

____
Rodger Liddle

Dissertation submitted in partial fulfillment of
the requirements for the degree of Doctor
of Philosophy in the Department of
Pharmacology and Cancer Biology in the Graduate School
of Duke University

2015

ABSTRACT

Characterization of the Role of Transferrin receptor 1 (Tfr1) in the Intestinal Epithelium, Pancreas, and Skin

by

Alan Chen

Department of Pharmacology and Cancer Biology
Duke University

Date:________________________
Approved:

____
Nancy Andrews, Supervisor

____
David Kirsch

____
Terry Lechler

____
Rodger Liddle

An abstract of a dissertation submitted in partial
fulfillment of the requirements for the degree
of Doctor of Philosophy in the Department of
Pharmacology and Cancer Biology in the Graduate School of
Duke University

2015

Abstract

Characterization of the role of transferrin receptor 1 (Tfr1) in the intestinal epithelium, pancreas and skin

Transferrin receptor 1 (Tfr1) serves as a receptor for transferrin, an iron-binding protein in the blood, in its canonical role of iron assimilation. Tfr1 is expressed ubiquitously in many tissues and is believed to be required for iron uptake by most cells (*1*).

The Tfr1 global knockout mouse highlights the requirement for Tfr1 in erythrocyte precursors (*2*). The erythron is the tissue with the highest iron requirement, to enable hemoglobin production (*3*). Tfr1-null embryos die by embryonic day 12.5 with anemia, which has been assumed to cause lethality of the knockout mice. Due to the embryonic lethality of the mice, the role of Tfr1 has not been well characterized in other tissues *in vivo*. This thesis examines the role of Tfr1 in other tissues through the generation and characterization of conditional knockout mouse models of Tfr1 deletion in the intestinal epithelium, pancreas, and skin.

Tfr1 is expressed on the basolateral surface of proliferating cells in the intestinal epithelium. Deletion of Tfr1 specifically in the intestinal epithelium resulted in the loss of intestinal epithelial homeostasis, loss of proliferation, lipid accumulation, gene expression indicating epithelial to mesenchymal transition of intestinal epithelial cells, and early neonatal lethality. These phenotypes were mostly alleviated by forced expression of a mutant Tfr1 allele which is unable to bind to iron-loaded transferrin,

suggesting that Tfr1 has a novel role independent of its canonical iron-assimilatory ability.

Deletion of Tfr1 in the pancreas resulted in juvenile death due to perturbed homeostasis of both endocrine and exocrine tissues, resulting in symptoms associated with pancreatitis and diabetes. No diabetic phenotype was detected in the conditional knockout mouse model of Tfr1 deletion specifically in β-cells, suggesting that the primary effect of the loss of Tfr1 was limited to the exocrine tissue.

Deletion of Tfr1 in the epidermis of the skin caused neonatal lethality with abnormal hair follicle morphology and a significant reduction in dermal adipocytes.

These results indicate that the loss of Tfr1 has pleiotropic effects, depending on the cell type affected. Furthermore, Tfr1 appears to have non-canonical functions in the intestinal epithelium, a novel discovery.

Dedication

This body of work is dedicated to my parents, Mr. and Mrs. David and Jiyan Chen. Their sacrifices gave me the opportunity to be the person that I am today.

Contents

List of Figures

Acknowledgements

Thank you to my wonderful mentor Dr. Nancy Andrews and my entire committee for their support. Thanks to my committee members for their advice and help with numerous reagents. Thanks for Adriana Donovan and Renee Ned for their work on the *Tfr1*$^{fl/fl}$*;Villin-Cre* mouse. Finally, thank you to Michael Landowski for his work on the skin histology.

1. General Introduction

Iron, as an ion or in the form of heme or Fe-S clusters, is required for the function of various essential proteins such as hemoglobin, ribonucleotide reductase, and components of the electron transport chain. Free iron molecules are highly catalytic and can promote the creation of reactive oxidative species, resulting in damage to proteins, lipids, and nucleic acids. At physiological conditions, iron present in the Fe(III) form, is highly insoluble in aqueous solutions. To alleviate these issues, transferrin, a very abundant plasma protein, is able to bind and stabilize iron in the serum. Iron-loaded transferrin binds to Tfr1 at the cell surface and is internalized through receptor-mediated, clathrin-dependent endocytosis. As the pH within the early endosome decreases to ~5.5, iron is released from transferrin and trafficked across the endosomal membrane. Transmembrane transport is carried out by the iron transporter DMT1 in erythroid precursors and possibly other cell types. Apo-transferrin, complexed with Tfr1, is recycled back to the cell surface. Due to the higher extracellular pH of ~7.4, apo-transferrin dissociates from Tfr1 and reenters the serum for the next around of iron acquisition. This process is termed the transferrin cycle.

Tfr1 is a homodimer capable of binding up to two molecules of transferrin, while transferrin is capable of bind up to two molecules of iron. Tfr1 is a 90-100 kDa glycoprotein which is post-transcriptionally regulated in an iron-dependent manner in non-erythroid tissues. In the case of low intracellular iron, iron regulatory proteins bind to iron response elements at the 3'UTR of the *Tfr1* mRNA, inhibiting degradation of the transcript and increasing levels of Tfr1 for iron acquisition. In the case of high intracellular iron, these iron regulatory proteins are unable to bind to the iron response elements, allowing degradation of the transcript and a resulting decrease in Tfr1 protein.

2. The transferrin receptor is essential for intestinal homeostasis

2.1 Introduction

Tfr1 is a cell surface protein which binds and takes up iron-loaded transferrin from the serum through receptor-mediated endocytosis (the transferrin cycle), and is critical for iron acquisition by erythroid precursors. Tfr1 is expressed at low levels in most tissues, but more highly expressed in the placenta, erythroid precursors, activated lymphocytes, osteoclasts, microglia, intestinal crypt cells, cultured cells and many cancers (*4*). We previously generated and characterized global *Tfr1-/-* mouse embryos. *Tfr1-/-* mice developed severe anemia due to impaired proliferation of erythroid precursors, and died by embryonic day 12.5. We further showed that hematopoietic cells require Tfr1 to develop but most other tissues appeared not to require it (*5*). Additionally, mice with severe deficiency of the ligand, transferrin, accumulated iron in non-hematopoietic tissues (6). Together these results demonstrated that Tfr1 is not universally required for iron uptake.

Diverse, non-canonical functions of Tfr1 and homologous proteins have also been elucidated. In the liver Tfr1 interacts with Hfe, an atypical major histocompatibility class I-like protein that is mutated in most patients with hemochromatosis, to sequester Hfe and thus modulate expression of hepcidin, an important iron-regulatory hormone (*7*). In celiac disease, Tfr1 is improperly localized the apical surface of mature enterocytes where it can bind to and transport dietary IgA (*8*). Tfr1 can also serve as a cell surface receptor for pathogenic New World hemorrhagic fever arenaviruses (*9*) and parvoviruses (*10*), which make use of its endocytic cycle. Tfr1 has a non-functional carboxypeptidase domain of uncertain function and two close mammalian homologs – Tfr2, which can function as a transferrin receptor but appears to primarily act as a sensor of iron stores (*11*) and Folh1, a folate hydrolase (*12*) -- as well as several other, more distant homologs (*13*). Tfr1 has been implicated in T cell receptor signaling (*14,15*), though its role remains uncertain.

Endocytosis of Tfr1 requires a cytoplasmic tetrapeptide internalization sequence (^{20}YTRF^{23}) (*16*). Tfr1 endocytosis has been described as constitutive because it is not ligand-dependent, but it is regulated by Src phosphorylation of dynamin and cortactin (*17*). Interestingly, Src also phosphorylates the tyrosine residue in the endocytosis motif (*18*). This promiscuous motif has also been shown to be the interaction site for the autophagy protein Gabarap (*19*), which in turn interacts with the anti-apoptotic protein Bcl2 (*20*), and also for the exosome protein Alix [(Pdcd6ip) (*21*).

Tfr1 is localized on the basolateral surface of intestinal epithelial cells (IECs) in the crypts (*22*), the proliferative niche of the intestinal epithelium (*23*). Binding of transferrin to the basolateral surface of IECs was decreased through dietary iron overload in mice (*24*). Conversely, binding was increased during iron deficiency, suggesting that Tfr1 might have a role in maintaining iron homeostasis within IECs. In an attempt to better understand its function in the intestine, we developed conditional knockout mice using Cre recombinase expressed throughout the intestinal epithelium. These mutant mice had a severe, early lethal phenotype that appears to be from loss of a novel function of Tfr1, not involving iron assimilation.

2.2 Materials and methods

Mouse breeding

Tfr1$^{IEC\text{-}KO}$ mice were generated by crossing *Tfr1*$^{fl/fl}$ mice (129 background) with *villin-Cre* mice (129 background). Resulting progeny were intercrossed to generate *Tfr1*$^{fl/+}$; *villin-Cre* mice in the F2 generation, which were used as parents to produce the F3 generation used in experiments.

Tfr1$^{iIEC\text{-}KO}$ mice were generated by crossing *Tfr1*$^{fl/fl}$ mice (129 background) with *villin-CreERT2* mice (Bl/6 background). Resulting progeny were intercrossed to generate *Tfr1*^{flfl}; *villin-CreERT2* mice in the F2 generation, which were used as parents to produce the F3 generation used in experiments.

Tfr1$^{IEC\text{-}KO}$*;Rosa26*$^{Tfr1R654A/+}$ mice were generated by crossing *Tfr1*^{flfl}; *villin-Cre* mice (129 background) with *Rosa26*$^{Tfr1R654A/+}$mice (129 background). Resulting progeny were intercrossed to generate *Tfr1*^{flfl}; *villin-Cre* mice in the F2 generation, which were used as parents to produce the F3 generation used in experiments.

Wildtype controls for both mouse strains were *Tfr1*$^{fl/fl}$ or *Tfr1*$^{fl/+}$,which have no phenotype.

Histology

Duodenal or colonic tissue was dissected from pups and fixed overnight in 10% formalin followed by 70% ethanol. Tissue pieces were embedded in paraffin and sectioned longitudinally. Hematoxylin and eosin staining was performed after sections were deparaffinized and rehydrated. Ki67 staining was performed was performed after antibody retrieval by boiling the slide in 10mM sodium citrate buffer pH 6.0.

Immunofluorescence and Oil-Red-O staining

Duodenal or colonic tissue was dissected from pups, embedded in OCT media, and snap frozen in liquid nitrogen. Duodenal or colonic tissue was then sectioned longitudinally, fixed with ice cold acetone for 15 minutes, and permeabilized with 0.1% Tween-20. Sections were stained with mouse anti-human Tfr1 (Invitrogen), goat anti-mouse Alexafluor 488 secondary (Life Technologies), and DAPI. Sections were also stained with Oil-Red-O to assess neutral lipid content.

Tamoxifen injection

Tamoxifen injections were performed through daily intraperitoneal injections, with a single dose (3mg/40g body weigh) for 5 days.

Iron-dextran injection

A single dose of iron-dextran (1mg) was performed through daily intraperitoneal injection, followed by tamoxifen injection after 5 days.

Microarray

Crypt-enriched IECs were harvested from duodenum and proximal colon as previously described. RNA extraction was performed using QIAGEN RNeasy kit and used with Genechip Mouse Genome 430 2.0 Array (Affymetrix).

Statistical analysis

P-values were determined for RT-PCR values by student's t-test. Error bars represent standard error of the mean.

2.3 Results

Neonatal lethality in mice with conditional deletion of *Tfr1* in IECs

In order to investigate the role of Tfr1 in IECs and to circumvent the embryonic lethality of the global *Tfr1-/-* mice, we generated a IEC-specific conditional knockout mouse model (*Tfr1*$^{IEC\text{-}KO}$) by crossing *Tfr1*$^{fl/fl}$ mice with *villin-Cre* transgenic mice (*25*). The *villin-Cre* transgene is known to be expressed in all IECs, including stem cells, by embryonic day 12.5 (E12.5). The resulting *Tfr1*$^{IEC\text{-}KO}$ pups were born in Mendelian ratios. *Tfr1*$^{IEC\text{-}KO}$ pups were indistinguishable from their wild type (*Tfr1*$^{fl/fl}$ and *Tfr1*$^{fl/+}$) littermates at birth. However, they failed to thrive and were severely runted by postnatal day 1 (P1) (**Figure 1A**). Lethality was observed in *Tfr1*$^{IEC\text{-}KO}$ pups beginning from P1 to P3, at which time 100% of the mice had died (**Figure 1B**). The stomachs of P1 *Tfr1*$^{IEC\text{-}KO}$ pups were distended and full of milk. Milk was also detected in the intestinal lumen (not shown and **Figure 1C**). The lengths of both the intestine and colon were shorter in *Tfr1*$^{IEC\text{-}KO}$ pups by P1. Histology of other tissues appeared normal (not shown). An enriched population of intervillous IECs and colonic crypts was isolated and used to validate loss of Tfr1 transcript and protein (**Figure 1D, E**). The small amount of Tfr1 detected can likely be attributed to non-IEC contaminating cells collected during the isolation process.

Conditional deletion of *Tfr1* in IECs results in the loss of intestinal epithelial homeostasis and proliferation

To confirm previous reports of Tfr1 localization in the intestinal epithelium, and to determine whether Tfr1 was present in the intestines of *Tfr1*$^{IEC\text{-}KO}$ mice, we examined duodenal sections for immunofluorescence using an anti-Tfr1 antibody. As expected, Tfr1 was found be enriched on the basolateral surface of P0 IECs in control mice, with the highest expression localized to cells residing in the intervillous region, but it was undetected in *Tfr1*$^{IEC\text{-}KO}$ IECs (**Figure 2A**).

Hematoxylin and eosin (H&E) staining of duodenal sections revealed a severe disruption in the *Tfr1*$^{IEC\text{-}KO}$ epithelium by P1 (**Figure 2B)**. The disruption was characterized by blunted villi, shallow intervillous regions, edema in the lamina propria, subepithelial neutrophilic infiltration, and enlarged vacuole-like structures in the IECs. Given the severe defects in epithelial integrity, it is likely that some of these phenotypes are either triggered or exacerbated by microbial infiltration following the loss of barrier function and subsequent inflammatory response. Loss of proliferation in intervillous IECs was shown through Ki67 staining.

Tfr1 is required for adult intestinal epithelial homeostasis and proliferation

We considered the possibility that Tfr1 is important for early development of the intestine, but dispensable in mature animals. We developed inducible Tfr1 conditional knockout mice (*Tfr1*$^{iIEC\text{-}KO}$) by crossing *Tfr1*$^{fl/fl}$ animals with transgenic mice carrying the tamoxifen-inducible *villin-CreERT2* allele to investigate the requirement of Tfr1 in the adult IECs. Adult mice were given a daily dose of tamoxifen through intraperitoneal (i.p.) injection for 5 days to induce deletion of *Tfr1* in IECs. The resulting *Tfr1*$^{iIEC\text{-}KO}$ mice developed severe diarrhea and weight loss as early as the 4th day of tamoxifen administration. Due to poor health, all of the *Tfr1*$^{iIEC\text{-}KO}$ mice treated with tamoxifen were euthanized 1 to 3 days after the last injection of tamoxifen (**Figure 3A**).

Much like the *Tfr1*$^{IEC\text{-}KO}$ phenotype, *Tfr1*$^{iIEC\text{-}KO}$ mice had distended stomachs full of chow with evidence of food in the intestinal tract (**Figure 3B**). H&E staining of *Tfr1*$^{iIEC\text{-}KO}$ duodenal sections showed blunted villi and subepithelial neutrophil infiltration (**Figure 3C**). Furthermore, Ki67 staining showed a reduction in the number of proliferating crypt IECs compared to tamoxifen-treated *Tfr1*$^{fl/fl}$ intestines and untreated intestines of both *Tfr1* genotypes (not shown).

Iron loading prior to *Tfr1* deletion in adult IECs does not rescue the phenotype

Other work from our lab has shown that administration of a large dose of iron dextran, to supersaturate circulating transferrin, results in iron loading of skeletal and cardiac muscle and rescue of muscle-specific Tfr1 conditional knockout mice (T Barrientos, W Xu and NCA, unpublished). This experiment was not feasible in *Tfr1*$^{IEC\text{-}KO}$ mice because they died so soon after birth. Instead, to examine whether similar iron-loading of IECs prior to Tfr1 loss could rescue *Tfr1*$^{iIEC\text{-}KO}$ mice, we treated *Tfr1*$^{iIEC\text{-}KO}$ adult mice with iron-dextran, then induced deletion of *Tfr1* with tamoxifen. The lifespans of the iron-loaded *Tfr1*$^{iIEC\text{-}KO}$ mice were not extended (**Figure 4A**). Similar to the non-iron-loaded *Tfr1*$^{iIEC\text{-}KO}$ mice, we observed diarrhea and body weight loss in iron-loaded *Tfr1*$^{iIEC\text{-}KO}$ mice in which *Tfr1* deletion was induced by tamoxifen (not shown). Similarly, the stomach was distended (**Figure 4B**). We confirmed that IECs of iron dextran-treated mice had increased iron content by measuring non-heme iron in intestinal scrapings (**Figure 4C**).

A novel function of Tfr1 rescues *Tfr1*$^{IEC\text{-}KO}$ lethality

The failure of iron overload to rescue IECs from deleterious effects of *Tfr1* deletion suggested that Tfr1 might be important for another function, rather than iron uptake. To investigate this possibility, we took advantage of mice expressing with an allele of *Tfr1* carrying a single missense mutation that preclude transferrin binding under the control of the ubiquitously expressed Rosa26 promoter (*26*). These mice were bred with the *Tfr1*$^{IEC\text{-}KO}$ mice to generate *Tfr1*$^{IEC\text{-}KO}$ mice which carried a single copy of the *Rosa26*^{Tfr1R654A} allele (*Tfr1*$^{IEC\text{-}KO}$;*Rosa26*$^{Tfr1R654A/+}$). We reasoned that, if the main role of Tfr1 in IECs is something other than to assimilate iron, then expression of *Rosa26*^{Tfr1R654A} might rescue the lethality of *Tfr1*$^{IEC\text{-}KO}$ mice. We found that the large majority of animals survived the neonatal period when unrescued *Tfr1*$^{IEC\text{-}KO}$ mice invariably died, and approximately 60% of the *Tfr1*$^{IEC\text{-}KO}$*;Rosa26*$^{Tfr1R654A/+}$ were alive at 2 months (**Figure 5A**). Those *Tfr1*$^{IEC\text{-}KO}$*;Rosa26*$^{Tfr1R654A/+}$ pups which did not survive beyond the neonatal period appeared to develop the same phenotype as *Tfr1*$^{IEC\text{-}KO}$ pups.

H&E staining of *Tfr1*$^{IEC\text{-}KO}$*;Rosa26*$^{Tfr1R654A/+}$ intestinal sections at 2 months showed normal intestinal architecture (**Figure 5B**). We did not see edema, enlarged vacuole-like structures, or subepithelial neutrophilic infiltration. Furthermore, proliferation of IECs residing in the intervillous regions was intact, as assessed by Ki67 staining. Taken together, these results suggest that Tfr1 plays a role in intestinal epithelial homeostasis and proliferation that is independent of its ability to bind and assimilate iron-transferrin.

Loss of Tfr1 in IECs induces genes associated epithelial-to-mesenchymal transition

To investigate the defect in IECs lacking Tfr1, we isolated P0 IECs from each of three *Tfr1*$^{fl/fl}$, *Tfr1*$^{IEC\text{-}KO}$, and *Tfr1*$^{IEC\text{-}KO}$*;Rosa26*$^{Tfr1R654A/+}$ mice and utilized microarray profiling to compare gene expression in the three genotypes. IEC samples were enriched for intestinal intervillous cells and crypts from the proximal colon. Principal component analysis done indicated that one of the three *Tfr1*$^{IEC\text{-}KO}$ samples was an outlier, and because our primary goal was to develop hypotheses we excluded it from the analysis here, but included it below. Results were initially analyzed by the Duke Microarray Shared Resource using Partek Genomics Suite 6.5, comparing *Tfr1*$^{IEC\text{-}KO}$ samples with

Tfr1$^{fl/fl}$ samples and with *Tfr1*$^{IEC\text{-}KO}$*;Rosa26*$^{Tfr1R654A/+}$. Strikingly, the only statistically significant differences between the two comparisons were in genes found on the Y chromosome (likely due to sex differences in the animals used) and in *Tfr1* itself, which was more highly expressed in the *Tfr1*$^{IEC\text{-}KO}$*;Rosa26*$^{Tfr1R654A/+}$ animals than in the controls (not shown). This was consistent with our conclusion that the mutant allele expressed from the *Rosa26* locus restored a necessary function of Tfr1.

We looked for informative patterns using Gene Set Enrichment Analysis [GSEA; (*27*,*28*)]. Genes upregulated at least 2 fold in *Tfr1*$^{IEC\text{-}KO}$ animals, compared to *Tfr1*$^{fl/fl}$ animals, included those associated with the adult tissue stem cell signature, the mesenchymal transition signature, axon guidance, cell adhesion and extracellular matrix interactions, along with many other similar associations. Transcriptional targets of Lef1, Foxo4, Nfat and Maz were very highly represented. Additionally, there was a highly significant association with targets of miRNAs known to regulate genes involved in the epithelial to mesenchymal transition (EMT), most notably of the miR-200b, miR-200c, miR-429 family. These results strong suggested that at least some cells within the mutant samples were undergoing EMT.

We compared expression of genes associated with EMT from all *Tfr1*$^{fl/fl}$, *Tfr1*$^{IEC\text{-}KO}$ and *Tfr1*$^{IEC\text{-}KO}$*;Rosa26*$^{Tfr1R654A/+}$ mice in a heat map (**Figure 6**). We observed marked upregulation of expression of EMT genes in two of the *Tfr1*$^{IEC\text{-}KO}$ mice compared to *Tfr1*$^{fl/fl}$ controls, but a much less striking pattern in the third mouse, which had been the outlier in principal component analysis. As noted earlier, there was variability in when the mutant mice died after birth (**Figure 5A**), and we speculate that the outlier mouse might have been developing the mutant phenotype later than the other two mice. EMT-associated genes upregulated 3 to 10 fold included well-characterized transcription factors that are activated early in EMT such as *Snai2, Zeb1, Zeb2* and *Sox4* (*29*), among others. During EMT, these transcription factors are capable of inducing expression of mesenchymal-associated cytoskeletal genes such as N-cadherin, vimentin, and alpha-smooth muscle actin, as well as extracellular matrix elements, such as fibronectin, collagens, and metalloproteases. These mRNAs were almost all markedly upregulated in our microarray data. Additionally, a large number of EMT-associated receptors, ligands, and signaling transducers including Tgfβ2, Tgfβ2 receptor, and multiple components of the Wnt, Notch, and Hedgehog signal transduction pathways were elevated at the mRNA transcript level.

$Tfr1^{IEC\text{-}KO}$;$Rosa26^{Tfr1R654A/+}$ rescued mice were much more similar to $Tfr1^{fl/fl}$ mice than $Tfr1^{IEC\text{-}KO}$ mice in their expression of EMT-related genes (**Figure 6**), consistent with the overall microarray data and corroborating that the protein expressed from the allele of *Tfr1* that cannot bind transferrin largely rescues the mutant phenotype. Once again this suggests a novel, non-canonical role for Tfr1 in IECs.

Lipid malabsorption in *Tfr1*$^{IEC\text{-}KO}$ intestinal epithelial cells

The pattern of genes downregulated 2-fold or more in *Tfr1*$^{IEC\text{-}KO}$ animals compared to *Tfr1*$^{fl/fl}$ and rescued animals was not as striking as the pattern of upregulated genes, but it was still informative. It included genes associated with arginine and proline metabolism, fatty acid metabolism, lysosomes, lipid and lipoprotein metabolism and transmembrane solute transport, along with other associations.

We had noted large, vacuole-like structures in H&E stained sections from *Tfr1*$^{IEC\text{-}KO}$ small intestine (**Figure 2B)**, and hypothesized that they might contain lipids. We examined the IECs by electron microscopy and found that these round, relatively homogeneous inclusions appeared to also be present in control animals, but were markedly enlarged in the mutant mice (**Figure 7A**). Some of the large inclusions appeared to be breaking through the apical membrane of enterocytes. However the number and size of similar, but smaller, inclusions in subepithelial tissue was indistinguishable between control and mutant mice. Oil-red-O staining (**Figure 7B**) confirmed that the large inclusions contained neutral lipid.

Dietary lipids are absorbed and assembled by IECs into chylomicrons, which are then released from the basolateral surface into the lamina propria for export into lacteal vessels (*30*). We noted that loss of the transcription factor pleomorphic adenoma gene-like 2 (Plagl2) in IECs similarly results in the accumulation of lipids in large vacuole-like structures within IECs and in the interstitial and subepithelial compartments of the intestine (31). Like *Tfr1*$^{IEC\text{-}KO}$ neonates, *Plagl2*$^{-/-}$ pups died within the first few days of life. Downregulation of cargo transport genes involved in sorting nexins and vacuolar trafficking was implicated in the *Plagl2*$^{-/-}$ phenotype. Downregulation of this set of genes may lead to improper chylomicron assembly and transport, resulting in lipid accumulation. Importantly, *Plagl2* mRNA was downregulated in *Tfr1*$^{IEC\text{-}KO}$ IECs, and we observed decreased mRNA for the same set of sorting nexin and vacuolar trafficking genes that were decreased in *Plagl2*$^{-/-}$ IECs and hypothesized to be part of the chylomicron packaging process [**Figure 7C** and (31)]. These results raise the possibility that Tfr1 is involved, directly or indirectly, in Plagl2-mediated lipid transport and processing. Consistent with other results, transcript levels showed partial restoration in *Tfr1*$^{IEC\text{-}KO}$*;Rosa26*$^{Tfr1R654A/+}$ IECs.

A quiescent stem cell signature in *Tfr1*$^{IEC\text{-}KO}$ IECs

Neither induction of EMT nor aberrant lipid transport easily explained the loss of proliferation observed in IECs lacking Tfr1 (**Figures 2B and 3C)**. We noted that the most strongly (16-fold) downregulated gene in mutant crypts, *2010317E24Rik*, encodes a protein now called Sapcd2 (suppressor of APC domain 2; also p42.3 and C9orf140 in humans), which contains a domain that is homologous to adenomatous polyposis coli (Apc), which regulates Wnt signaling and is mutated in many colon cancers (*32*). The function of this protein is not known, but recent reports, but it has been associated with gastric and colorectal cancer progression, and its depletion in cultured cells causes G2/M arrest (*33*) (*34, 35*). This may contribute to the failure of proliferation we observed in *Tfr1*$^{IEC-KO}$ crypts.

In addition, genes downregulated in *Tfr1*$^{IEC-KO}$ IECs showed a significant association with targets of the Let-7 family of miRNAs. Let-7 overexpression leads to a decrease in cell cycle progression (*36*). There was also an association with miR-489**,** which has been shown to maintain muscle stem cell quiescence (*37*), miR-125a, which controls hematopoietic stem cell numbers (*38*) and miR-125b, which is induced by Snail through Wnt signaling and increases the cancer stem cell population (*39*). Together, these results support the idea that stem cells have become quiescent in *Tfr1*$^{IEC-KO}$ intestinal epithelium.

Plagl2, already mentioned, is targeted by multiple miRNAs that are significantly associated with down regulated genes in our dataset. Interestingly, the start of the *Plagl2* mRNA is approximately 100 bp away from the start of *Pofut1*, which is similarly downregulated, suggesting that they might share a promoter. Pofut1 is an O-fucosylating enzyme that acts on EGF repeats to modulate signaling. Along with several other genes, *Plagl2* and *Pofut1* are amplified in many human tumors; Plagl2 induces genes involved in Wnt signaling to block differentiation and promote proliferation (*40*). Decreased *Plagl2* expression may contribute to the decreased proliferation we have observed in our mutants.

We noted that a variety of known stem cell markers – *Kit, Thy1, Prom1 (Cd133), Cd34, Cd44, Fabp7, Ly6a (Sca1), Ndn, Dclk1* – were strongly upregulated in *Tfr1*$^{IEC\text{-}KO}$ IECs. Considering the increased expression of these stem cell genes, we infer that at least some *Tfr1*$^{IEC\text{-}KO}$ IECs have entered a quiescent stem cell state.

2.4 Discussion

While it is well established that Tfr1 is important for iron acquisition by erythroid cells, the requirement of Tfr1 and its roles in most other tissues, including the intestinal epithelium, has not been characterized. In this report we have demonstrated that Tfr1 is required for IEC proliferation and homeostasis in both developing and adult intestine. Animals lacking Tfr1 in the intestinal epithelium died within the first three days of life, with severe disruption of epithelial integrity, impaired proliferation and lipid-laden IECs. Enforced iron overload did not ameliorate the mutant phenotype, suggesting that the cells were not simply iron deficient. Rather, transgenic expression of a mutant allele of Tfr1 that is unable to bind to iron-loaded transferrin fully rescued most $Tfr1^{IEC\text{-}KO}$ mice. This raises the possibility that Tfr1 possesses a novel, non-canonical function in IECs that does not involve (or at least does not require) iron uptake.

There were three sub-phenotypes which, together, appeared to cause the epithelial disruption and early lethality: epithelial-mesenchymal transition, interrupted lipid trafficking, and impaired proliferation in the generative crypts. While all three sub-phenotypes were striking, we are not certain how loss of Tfr1 caused them or how they are linked to each other.

Microarray analysis of $Tfr1^{fl/fl}$, $Tfr1^{IEC\text{-}KO}$, and $Tfr1^{IEC\text{-}KO}$;$Rosa26^{Tfr1R654A/+}$ IECs revealed candidate regulatory networks which could explain the pleiotropic effects of the loss of Tfr1, give insight into its potential non-canonical mechanisms, and provide an explanation to the lethality. *Tfr1* deletion induced upregulation of a wide range of EMT-associated genes that have been well characterized in cells that have undergone EMT both *in vivo* and *in vitro*. The massive upregulation of many EMT-associated genes including early EMT initiators such as Snail2, Zeb1, and Zeb2 in *Tfr1$^{IEC\text{-}KO}$* P0 IECs implicates the involvement of Tfr1 in suppressing the initiating steps of EMT in the intestinal epithelium. The wide range of upregulated EMT-associated genes also suggests a cell fate switch that could possibly lead to the breakdown of the barrier function of the intestinal epithelium, contributing to the phenotype of the *Tfr1$^{IEC\text{-}KO}$* mice.

Both *Tfr1$^{IEC\text{-}KO}$* and *Plagl2$^{-/-}$* mice show a similar histological feature of abnormal lipid accumulation in the intestines. Both mutants have also downregulated a common set of sorting and transport molecules, which could impair chylomicron assembly and transport or other elements of lipid processing. Because *Plagl2* was downregulated in *Tfr1$^{IEC\text{-}KO}$* IECs, Tfr1 may play a role in Plagl2-mediated lipid processing and transport in the intestine. Interestingly, *Tfr1* deletion in older *Tfr1$^{iIEC\text{-}KO}$* mice did not result in abnormal lipid accumulation in IECs, lamina propria, or subepithelial compartments. This could possibly be due to the ingestion of lipid-rich milk in neonates overloading the impaired chylomicron processing machinery.

We showed that *Tfr1$^{IEC\text{-}KO}$;Rosa26$^{Tfr1R654A/+}$* IECs were able to largely correct all of the phenotypic and genotypic abnormalities observed in *Tfr1$^{IEC\text{-}KO}$* mice. The *Rosa26$^{Tfr1R654A/+}$* transgene encodes a Tfr1 molecule that differs from endogenous Tfr1 by a single missense mutation that disrupts extracellular transferrin binding, but leaves the rest of the molecule intact. This indicated that some function of Tfr1, apart from its role in iron uptake, was essential for intestinal homeostasis.

Considering the pleiotropic effects of loss of wild type Tfr1, we speculate that its essential role in IECs involves signal transduction. There is evidence that Tfr1 may have a signal transduction role. It has been identified as the cellular target of gambogic acid (GA), a natural compound that rapidly induces apoptosis (*41*). The binding site for GA on Tfr1 was shown to be distinct from that of transferrin. GA inhibits Tfr1 internalization, and the effect of GA apparently involves a signaling function, rather than the iron uptake function, of Tfr1. The nature of this signaling is unclear, though it was recently reported that phosphorylation of Tfr1 residue ^{20}Y by Src decreases apoptosis and promotes cancer cell survival, and Tfr1 mutants at ^{20}Y were more susceptible to GA (*42*).

GA was shown to inhibit Stat3 phosphorylation through activation of the phosphatase Shp-1, also known as Ptpn6 (*43*). This is particularly intriguing because shortly after cytokine induction, most activated Stat3 has been reported to be resident in early endosomes that also contain Tfr1, and inhibitors of the endocytic pathway blocked Stat3 transcriptional regulation (*44*). However, while these results suggest that Tfr1 may have a signaling role, possibly involving Stat3, there is much more work to be done to determine whether is pertinent to our observations in mice lacking Tfr1 in the intestinal epithelium.

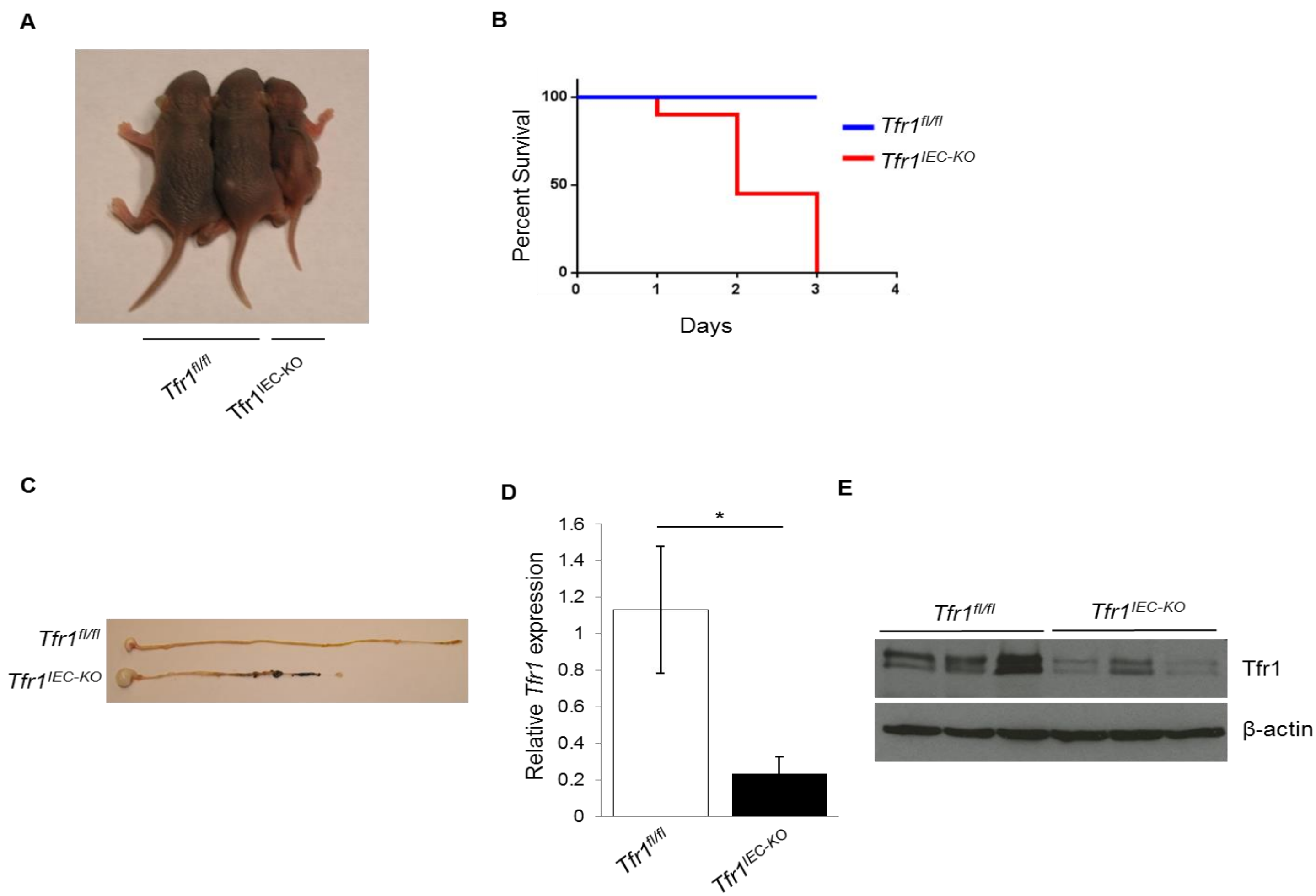
A
Tfr1fl/fl
Tfr1IEC-KO
B
Percent Survival
100
50
0
0
1
2
3
4
Days
Tfr1fl/fl
Tfr1IEC-KO
C
Tfr1fl/fl
Tfr1IEC-KO
D
Relative Tfr1 expression
1.6
1.4
1.2
1
0.8
0.6
0.4
0.2
0
*
Tfr1fl/fl
Tfr1IEC-KO
E
Tfr1fl/fl
Tfr1IEC-KO
Tfr1
β-actin

Figure 1. Phenotype of *Tfr1*$^{IEC\text{-}KO}$ mice.

(A) *Tfr1*$^{fl/fl}$ and *Tfr1*$^{IEC\text{-}KO}$ neonates at P1.

(B) Kaplan-Meier survival curves of *Tfr1*$^{fl/fl}$ (blue, n=12) and *Tfr1*$^{IEC\text{-}KO}$ (red, n=12) neonates. *Tfr1*$^{fl/fl}$ mice lived until sacrifice.

(C) Stomach (left), small intestine, and colon at P1.

(D) qRT-PCR comparing *Tfr1* expression in P0 *Tfr1*$^{fl/fl}$ (n=4) and *Tfr1*$^{IEC\text{-}KO}$ (n=6) IECs normalized by *β-actin* expression (*P<0.05).

(E) Western blot of P0 *Tfr1*$^{fl/fl}$ and *Tfr1*$^{IEC\text{-}KO}$ IEC lysates probed with Tfr1 or β-actin.

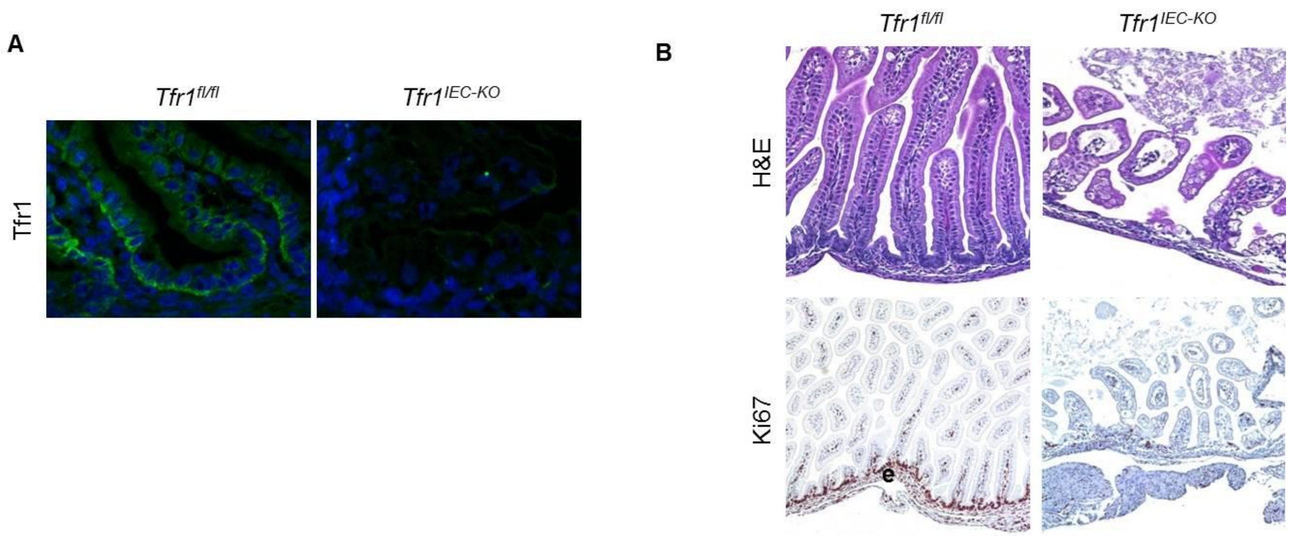
A
Tfr1^fl/fl
Tfr1^IEC-KO
Tfr1
B
Tfr1^fl/fl
Tfr1^IEC-KO
H&E
Ki67
e

Figure 2. Tfr1 is required for homeostasis in the developing intestinal epithelium.

(A) Immunofluorescence localization of Tfr1 (green) and DAPI (blue) in P1 duodenal sections. Tfr1 is found at on basolateral surface of intervillous control IECs but absent from *Tfr1*$^{IEC\text{-}KO}$ IECs.

(B) H&E staining of P1 duodenal sections showing blunted villi, smaller intervillous regions, and edema in *Tfr1*$^{IEC\text{-}KO}$ mice. Ki67 staining of P1 duodenal sections showing reduced proliferation in *Tfr1*$^{IEC\text{-}KO}$ mice.

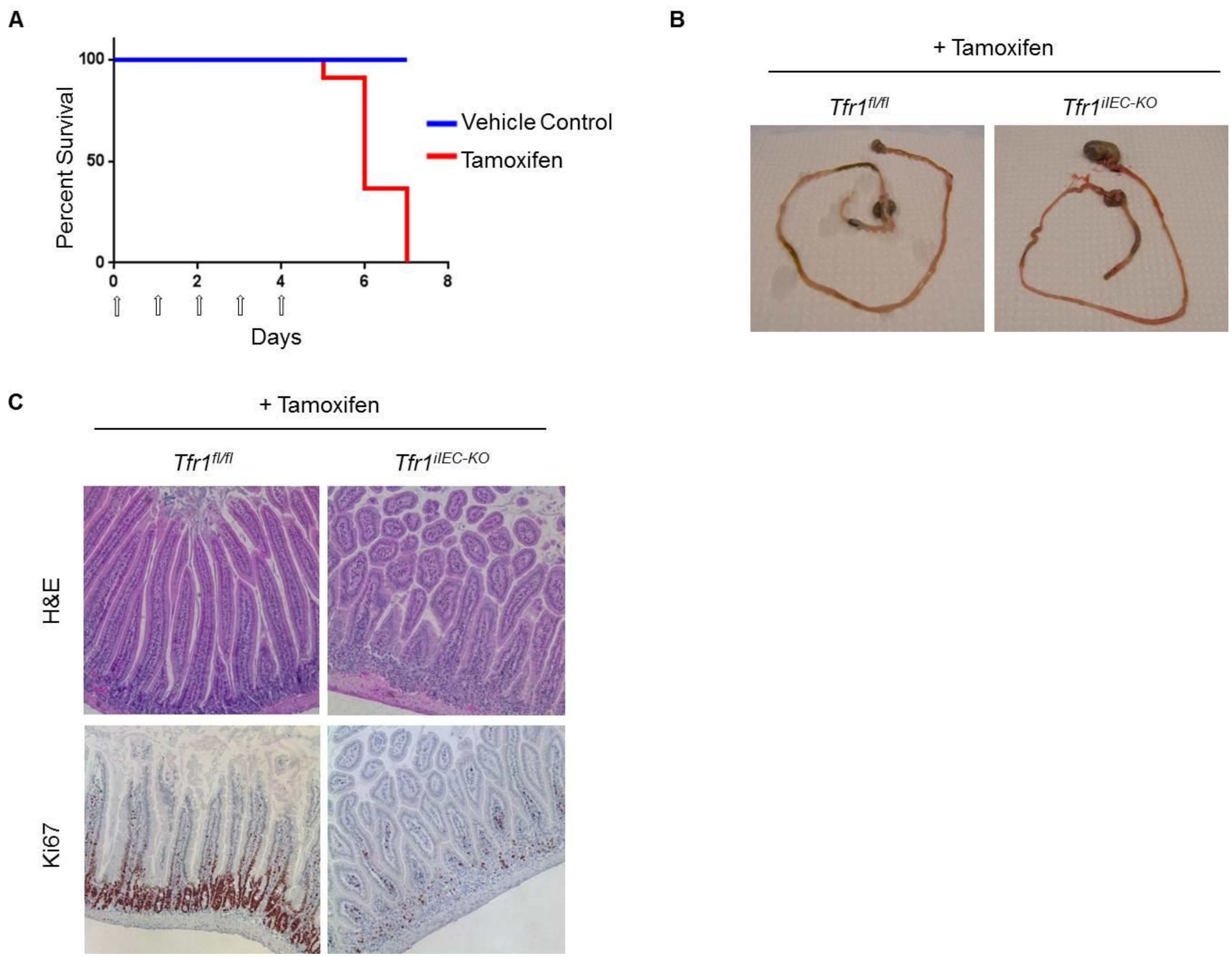
A
100
50
0
Percent Survival
0
2
4
6
8
Days
Vehicle Control
Tamoxifen
B
+ Tamoxifen
Tfr1fl/fl
Tfr1iIEC-KO
C
+ Tamoxifen
Tfr1fl/fl
Tfr1iIEC-KO
H&E
Ki67

Figure 3. Tfr1 is required for adult intestinal epithelial homeostasis.

(A) Kaplan-Meier survival curves of 2 month old control (n=10) and tamoxifen-treated *Tfr1*$^{iIEC\text{-}KO}$ mice (n=10). Daily injections of tamoxifen were given as indicated (white arrows).

(B) Stomach, intestine, and colon of tamoxifen-injected control and *Tfr1*$^{iIEC\text{-}KO}$ mice.

(C) H&E staining of duodenal sections showing disruption of the intestinal epithelium in adult *Tfr1*$^{iIEC\text{-}KO}$ mice with blunted villi and neutrophilic infiltration. Ki67 staining of adult duodenal sections showing a reduction of proliferating IECs in *Tfr1*$^{iIEC\text{-}KO}$ mice.

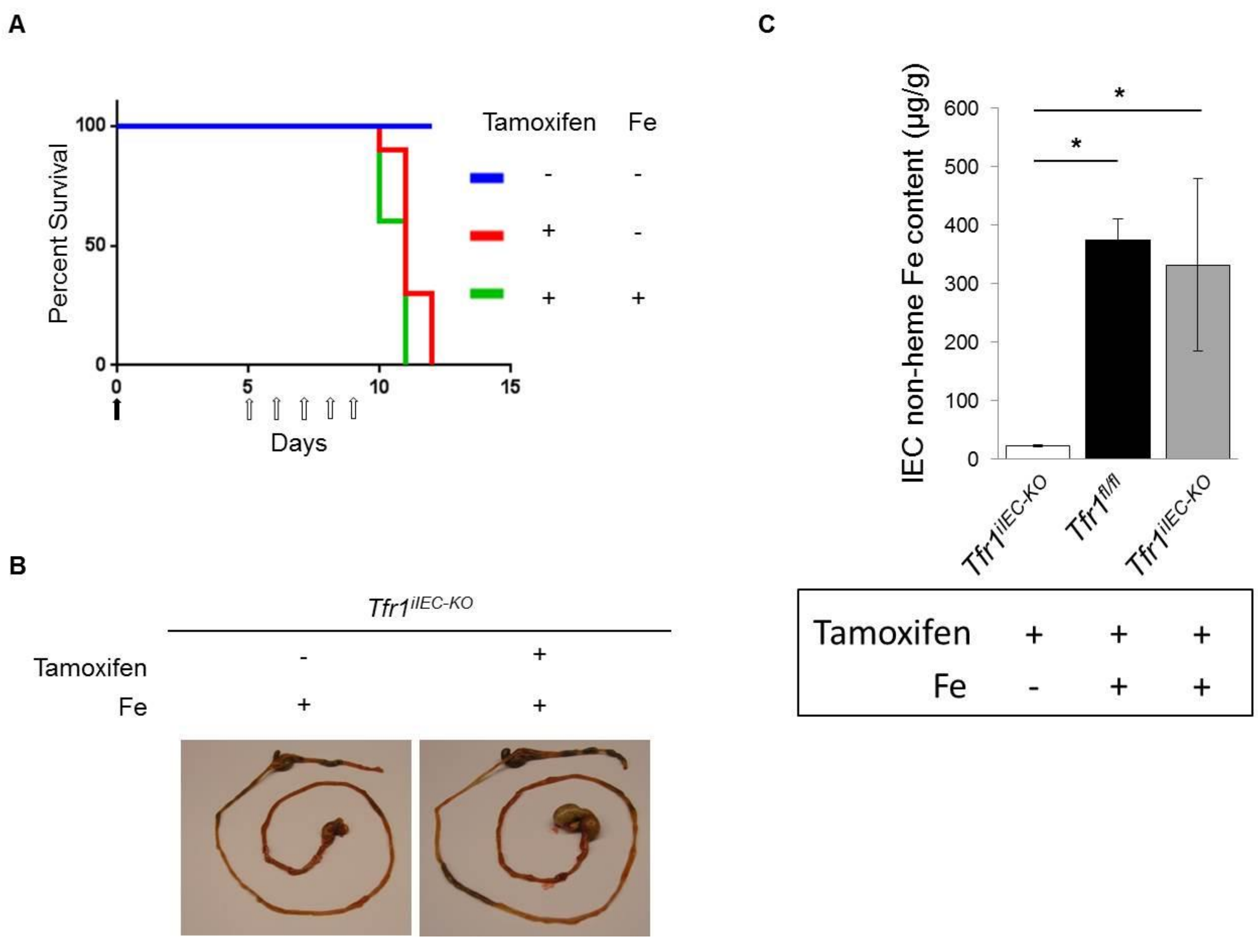
A
100
50
0
Percent Survival
0
5
10
15
Days
Tamoxifen
Fe
-
-
+
-
+
+
B
Tfr1iIEC-KO
Tamoxifen
Fe
-
+
+
+
C
IEC non-heme Fe content (µg/g)
600
500
400
300
200
100
0
*
*
Tfr1iIEC-KO
Tfr1fl/fl
Tfr1iIEC-KO
Tamoxifen + + +
Fe - + +

Figure 4. Iron-loading does not restore viability in adults.

(A) Kaplan-Meier survival curves of iron-loaded 2 month old mice treated with tamoxifen to delete *Tfr1*. A single dose of iron-dextran was given (black arrow). Five days later, daily injections of tamoxifen were given as indicated (white arrows) to induce deletion of Tfr1. Results are from iron-loaded (n=8) and non-iron-loaded, tamoxifen-injected (n=6) control mice and iron-loaded, tamoxifen injected $Tfr1^{iIEC\text{-}KO}$ mice (n=8).

(B) Stomach (center), intestine, and colon of iron-loaded, tamoxifen-injected control and $Tfr1^{iIEC\text{-}KO}$ adult mice.

(C) Non-heme iron content of IECs taken from intestinal scrapings of iron-loaded and non-iron-loaded, tamoxifen-injected control mice and iron-loaded, tamoxifen injected $Tfr1^{iIEC\text{-}KO}$ mice.

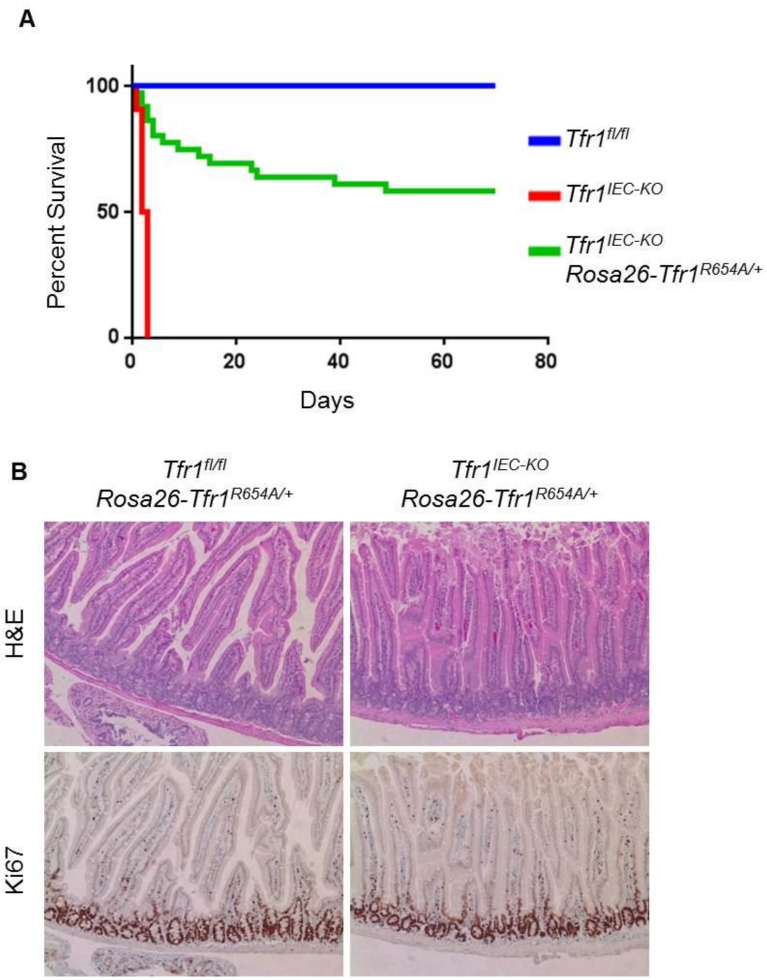

A
100
50
0
0
20
40
60
80
Percent Survival
Days
Tfr1fl/fl
Tfr1IEC-KO
Tfr1IEC-KO Rosa26-Tfr1R654A/+
B
Tfr1fl/fl Rosa26-Tfr1R654A/+
Tfr1IEC-KO Rosa26-Tfr1R654A/+
H&E
Ki67

Figure 5. $Tfr1^{R654A}$ rescues $Tfr1^{IEC\text{-}KO}$ mice.

(A) Kaplan-Meier survival curves showing rescue of most $Tfr1^{IEC\text{-}KO}$;*Rosa26-*$Tfr1^{R654A/+}$ mice (n=45) versus $Tfr1^{fl/fl}$ mice (n=12) and $Tfr1^{IEC\text{-}KO}$ mice (n=12).

(B) H&E staining of duodenal sections from 2 month old $Tfr1^{fl/fl}$;*Rosa26-*$Tfr1^{R654A/+}$ and $Tfr1^{IEC\text{-}KO}$;*Rosa26-*$Tfr1^{R654A/+}$ mice showing rescue of epithelial integrity. Ki67 staining of P1 duodenal sections showing proliferating IECs in rescued crypts.

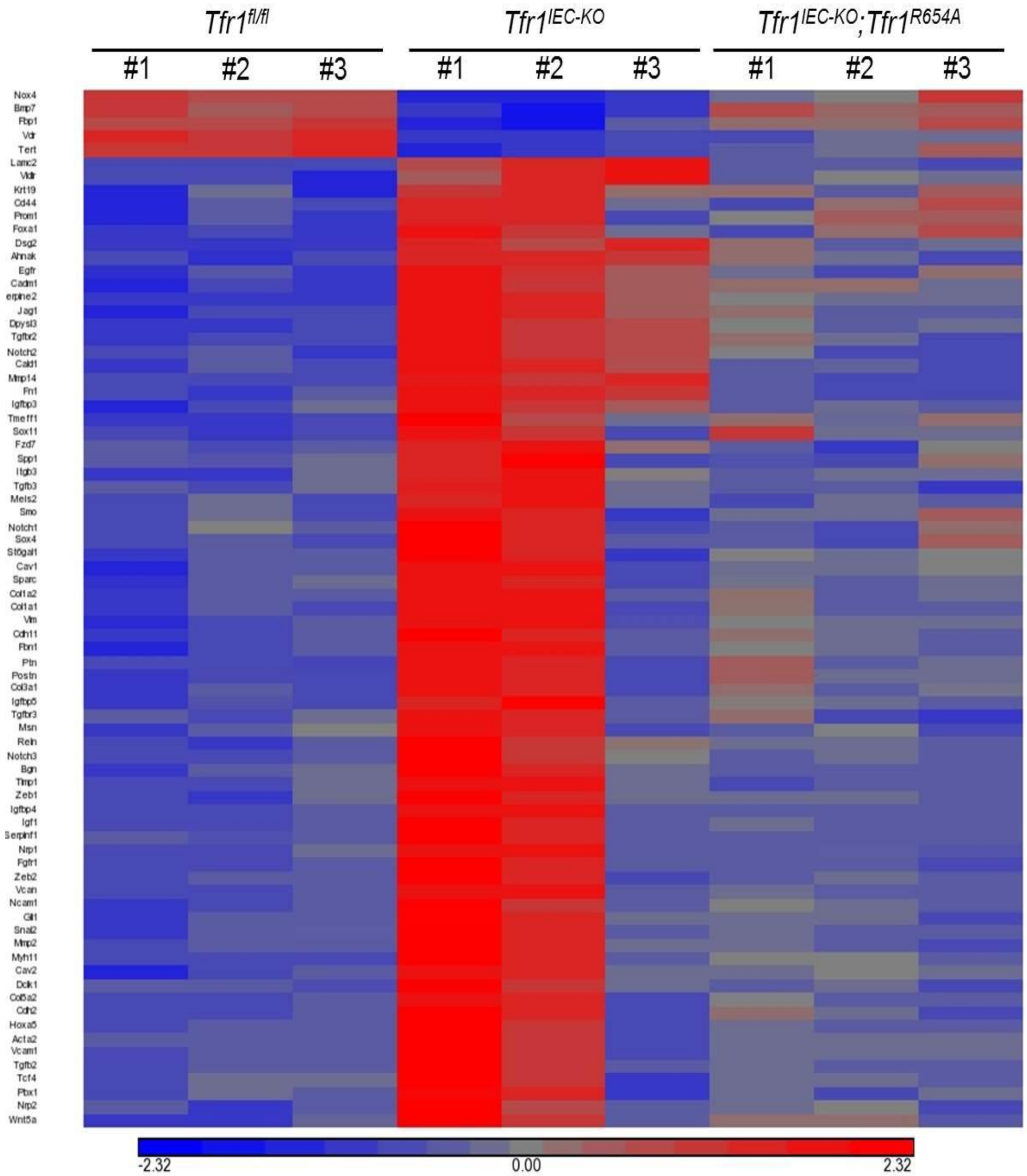
Tfr1fl/fl
Tfr1IEC-KO
Tfr1IEC-KO;Tfr1R654A
#1
#2
#3
#1
#2
#3
#1
#2
#3
Nox4
Bmp7
Fbp1
Vdr
Tert
Lamc2
Vldlr
Krt19
Cd44
Prom1
Foxa1
Dsg2
Ahnak
Egfr
Cadm1
erpine2
Jag1
Dpysl3
Tgfbr2
Notch2
Cald1
Mmp14
Fn1
Igfbp3
Tmeff1
Sox11
Fzd7
Spp1
Itgb3
Tgfb3
Meis2
Smo
Notch1
Sox4
St6gal1
Cav1
Sparc
Col1a2
Col1a1
Vim
Cdh11
Fbn1
Ptn
Postn
Col3a1
Igfbp5
Tgfbr3
Msn
Reln
Notch3
Bgn
Timp1
Zeb1
Igfbp4
Igf1
Serpinf1
Nrp1
Fgfr1
Zeb2
Vcan
Ncam1
Gli1
Snai2
Mmp2
Myh11
Cav2
Dclk1
Col5a2
Cdh2
Hoxa5
Acta2
Vcam1
Tgfb2
Tcf4
Pbx1
Nrp2
Wnt5a
-2.32
0.00
2.32

Figure 6. Induction of EMT-associated genes in *Tfr1*$^{IEC\text{-}KO}$ IECs.

Expression of EMT-associated genes ascertained by microarray profiling of *Tfr1*$^{fl/fl}$, *Tfr1*$^{IEC\text{-}KO}$, and *Tfr1*$^{IEC\text{-}KO}$;*Rosa26-Tfr1*$^{R654A/+}$ IECs.

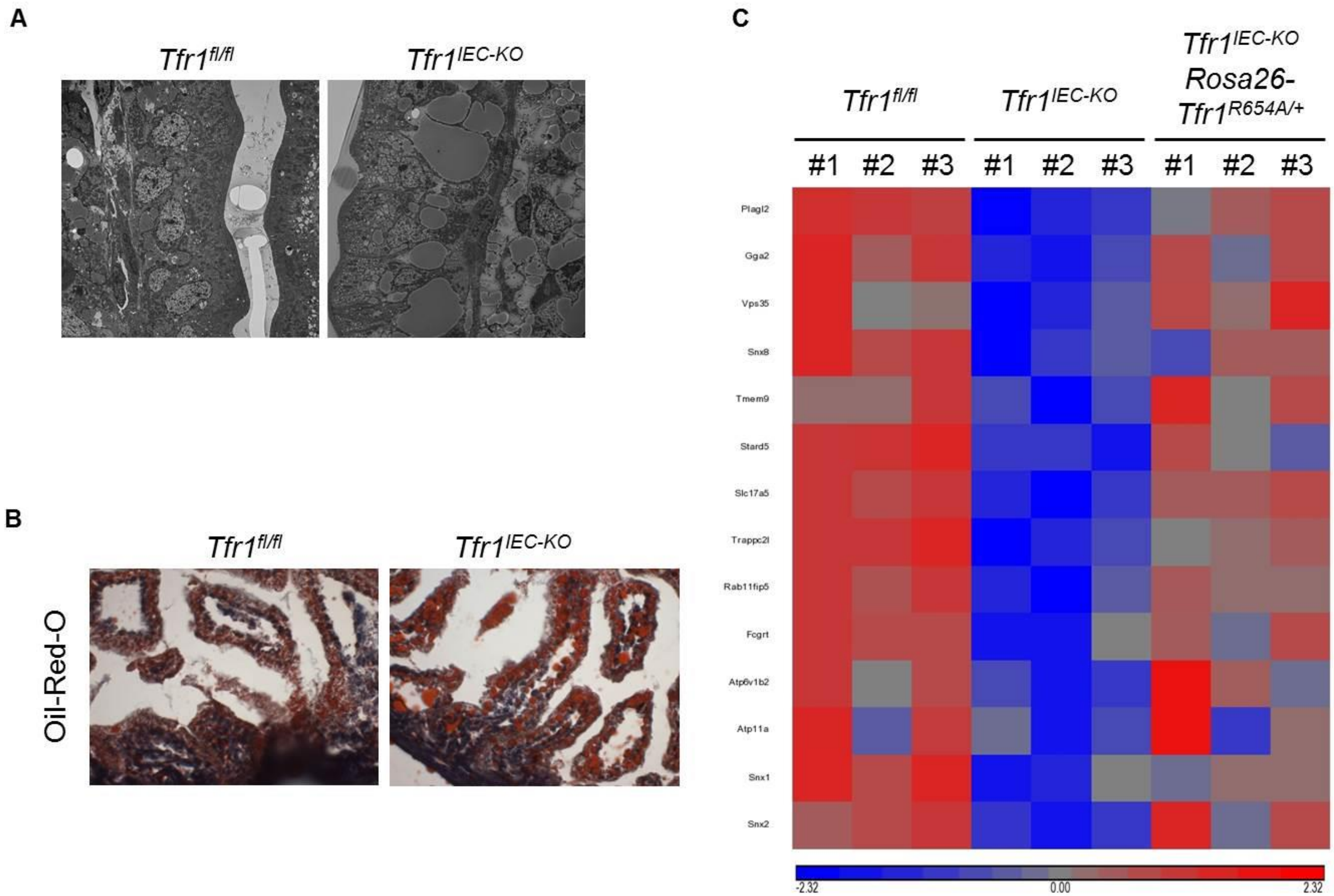
A
Tfr1fl/fl
Tfr1IEC-KO
B
Tfr1fl/fl
Tfr1IEC-KO
Oil-Red-O
C
Tfr1fl/fl
Tfr1IEC-KO
Tfr1IEC-KO Rosa26-Tfr1R654A/+
#1 #2 #3 #1 #2 #3 #1 #2 #3
Plagl2
Gga2
Vps35
Snx8
Tmem9
Stard5
Slc17a5
Trappc2l
Rab11fip5
Fcgrt
Atp6v1b2
Atp11a
Snx1
Snx2
-2.32
0.00
2.32

Figure 7. Altered lipid metabolism in *Tfr1$^{IEC\text{-}KO}$* IECs.

(A) Transmission electron microscopy showing large lipid droplets in IECs and smaller droplets in lamina propria of *Tfr1$^{IEC\text{-}KO}$* intestinal epithelium at P1.

(B) Oil-red-O staining of P1 intestinal epithelium confirming that droplets contain neutral lipids.

(C) Transport and sorting genes previously reported in *Plagl2$^{-/-}$* mice, selected from microarray profiles of *Tfr1$^{fl/fl}$*, *Tfr1$^{IEC\text{-}KO}$*, and *Tfr1$^{IEC\text{-}KO}$;Rosa26-Tfr1$^{R654A/+}$* IECs. These genes are hypothesized to be associated with intracellular secretory pathways disrupted in both *PlagL2$^{-/-}$* and *Tfr1$^{IEC\text{-}KO}$* intestinal epithelia.

3. The transferrin receptor in the pancreas

3.1 Introduction

The pancreas is a dual function organ comprised of endocrine and exocrine tissues. The exocrine tissue consists of acinar cells and ductal cells which secrete digestive enzymes into the pancreatic duct to pass into the duodenum. Acinar cells secrete enzymes such as trypsinogen, pancreatic lipase, phospholipase, DNAase and RNAse, and pancreatic amylase which aid in the breakdown and modification of proteins, triglycerides, phospholipids, nucleic acids, and starch respectively. These enzymes are mixed with bicarbonate produced by the ductal cells, which are epithelial cells that line the pancreatic duct, before the enzymes are released into the duodenum. The endocrine tissue is comprised of the islets of Langerhans, compact collections of cells interspersed between acinar clusters. Islets of Langerhans are comprised of α, β, γ, and δ, and ε-cells which secrete glucagon, insulin, pancreatic polypeptide, somatostatin, and ghrelin respectively (*45*). Systemic glucose homeostasis is regulated mainly by the two signaling peptides, glucagon and insulin. When blood glucose levels become low, glucagon is released by α-cells, signaling to the liver to convert stored glycogen into glucose and subsequently release glucose into the bloodstream. When blood glucose levels become high, insulin is released by the β-cells, signaling to skeletal muscle and fat tissue to absorb serum glucose and to halt the production and release of glucose by the liver. In type I and type 2 diabetes insulin insufficiency causes glucose to accumulate in the blood, resulting in hyperglycemia (*46*).

Damage to the pancreas due to genetic, immunologic, or environmental factors can have profound consequences on the digestive properties of the organ as well as the maintenance of bodily glucose homeostasis. Abuse of alcohol by humans can result acute pancreatitis, characterized by the inflammation and autodigestion of the tissue caused by improper release of digestive enzymes. Long term consumption of alcohol can result in chronic pancreatitis, in which permanent damage to both the exocrine and endocrine tissues, resulting in reduced digestive enzyme and insulin production and in fibrosis of the pancreas. In hereditary hemochromatosis, a disease characterized by increase in intestinal iron absorption and increased bodily iron stores, iron deposition in the pancreas can result in oxidative damage to β-cells leading to diabetes (*47*).

The characterization of Tfr1 localization in normal pancreatic tissue has been performed in normal, iron-deficient, and iron-loaded rat models. Tfr1 was detected in both acinar cells and in the islets of Langerhans of normal rats. The staining for Tfr1 increased in the iron-deficient rats and diminished in the iron-loaded rats (*48*). This suggests that Tfr1's role in pancreatic tissue may be iron acquisition and that iron-dependent regulation of Tfr1 expression remain intact.

3.2 Materials and Methods

Mouse breeding

$Tfr1^{Panc\text{-}KO}$ mice were generated by crossing $Tfr1^{fl/fl}$ mice (129 background) with *Pdx1-Cre* mice (Bl/6 background). Resulting progeny were intercrossed to generate

Tfr1$^{fl/+}$; *Pdx1-Cre* mice in the F2 generation, which were used as parents to produce the F3 generation used in experiments.

Tfr1$^{Beta\text{-}KO}$ mice were generated by crossing *Tfr1*$^{fl/fl}$ mice (129 background) with *ins2-Cre* mice (Bl/6 background). Resulting progeny were intercrossed to generate *Tfr1*^{flfl}; *Pdx1-Cre* mice in the F2 generation, which were used as parents to produce the F3 generation used in experiments.

Wildtype controls for both mouse strains were *Tfr1*$^{fl/fl}$ or *Tfr1*$^{fl/+}$,which have no phenotype.

Immunohistochemistry

Whole pancreas was dissected from 4 week old pups or 2 month old adults and fixed overnight in 10% formalin followed by 70% ethanol. Pancreases were embedded in paraffin and sectioned. Sections were deparaffinized and rehydrated, then stained with hematoxylin and eosin for general histology or Masson's trichrome stain for collagen.

Immunofluorescence

Whole pancreas was dissected from 4 week old pups and fixed overnight in 10% formalin followed by 70% ethanol. Pancreases were embedded in paraffin and sectioned. Sections were deparaffinized and rehydrated. Antibody retrieval was performed by boiling the slide in 10mM sodium citrate buffer pH 6.0. Staining for insulin was done with anti-guinea pig insulin primary antibody (Dako), goat anti-guinea pig Alexafluor 488 secondary antibody (Life Technologies), and DAPI.

Serum glucose measurements

Serum glucose levels were measured using a glucometer (Freestyle) and blood collected from tail nicks of 1 week, 2 week, 3 week, 4 week old, and 1 year old mice.

Serum insulin measurements

Retro-orbital bleeding was performed on 4 week old *Tfr1*$^{Panc\text{-}KO}$ mice using non-heparinized capillary tubes. Blood was allowed to clot, spun down, and supernatant was harvested. Serum insulin was measured using the rat/mouse insulin ELISA kit (Millipore).

Oil-Red-O staining of stool

Fecal smears were prepared from fresh stool harvested from 4 week old mice. Smears were dried overnight and stained with Oil-Red-O.

Statistical analysis

P-values were determined for blood glucose and serum insulin levels by student's t-test. Error bars represent standard error of the mean.

3.3 Results

Lethality in mice with conditional deletion of *Tfr1* in the pancreas

We generated a pancreas-specific conditional knockout (*Tfr1*$^{Panc\text{-}KO}$) mouse model by crossing *Tfr1*$^{fl/fl}$ mice with mouse *pdx1-Cre* transgenic mice. Pdx1, a homeobox gene, is required for embryonic pancreatic development and β-cell differentiation. The *Pdx1-Cre* transgene is mosaically expressed and has been detected in the pancreatic ductal epithelium, stomach, and duodenum in embryos and in β-cells in adults. In the pancreas, Tfr1 is expected to be deleted in exocrine, endocrine, and ductal epithelial cells, but in a mosaic fashion.

Tfr1$^{Panc\text{-}KO}$ mice were born in Mendelian ratios and were indistinguishable from their wildtype littermates at birth. Starting at 1 week, some *Tfr1*$^{Panc\text{-}KO}$ pups failed to thrive. Failure to thrive was accompanied by eventual weight loss, distended cecum, and smaller pancreas size.

Perturbation of exocrine and endocrine tissues in *Tfr1*$^{Panc\text{-}KO}$ pancreas

Hematoxylin and eosin staining was used to assess histology of exocrine and endocrine tissues of the *Tfr1*$^{Panc\text{-}KO}$ pancreas. *Tfr1*$^{Panc\text{-}KO}$ pancreas showed portions of disrupted tissue alongside tissue that was normal in appearance (**Figure 8**), likely due to the mosaic expression of Cre recombinase. Because of the mosaic expression, it is important to determine recombination efficiency and loss of Tfr1 protein in future works. Acinar morphology appeared abnormal, characterized by smaller acinar cells. Islets of Langerhans were smaller and more difficult to find in the affected tissue portions.

Loss of glucose and insulin homeostasis in *Tfr1$^{Panc\text{-}KO}$* mice

Due to the reduced number of islets observed in the *Tfr1$^{Panc\text{-}KO}$* mice, wildtype or *Tfr1$^{Panc\text{-}KO}$* pancreases were stained for insulin to detect if there was a corresponding decrease in the number of β-cells. Preliminary data suggest that islet numbers appear normal in unaffected portions of *Tfr1$^{Panc\text{-}KO}$* pancreas (data not shown). Unsurprisingly, insulin staining showed that there were very few β-cells in the *Tfr1$^{Panc\text{-}KO}$* pancreas (**Figure 9**). Serum insulin levels of *Tfr1$^{Panc\text{-}KO}$* mice were significantly lower than wildtype mice, showing that insulin homeostasis was lost perhaps due to the small number of insulin-producing β-cells left in the *Tfr1$^{Panc\text{-}KO}$* pancreas (**Figure 10**).

Because low insulin levels inhibit absorption of glucose by the skeletal muscle, hyperglycemia develops unless insulin levels are restored. Blood glucose levels were measured in wildtype and *Tfr1$^{Panc\text{-}KO}$* mice weekly from week 1 to week 4. Hyperglycemia was detected in some *Tfr1$^{Panc\text{-}KO}$* mice starting at 3 weeks (**Figure 11**). and, in those that did, the condition lasted for the remainder of their lives.

Tfr1$^{Panc\text{-}KO}$ mice exhibit characteristics of pancreatitis

The repeated damage to the pancreas in humans and mice with chronic pancreatitis results in the permanent destruction of tissue and the development of fibrosis. In order to detect the presence of fibrosis, wildtype and *Tfr1$^{Panc\text{-}KO}$* pancreases were stained for collagen. Collagen was detected in blood vessels in the wildtype pancreas as expected, however, collagen was also detected interspersed between acinar clusters in the

Tfr1$^{Panc\text{-}KO}$ pancreas (**Figure 12**). This is indicative of mild fibrogenesis following damage to the pancreatic tissue in the *Tfr1*$^{Panc\text{-}KO}$ mice.

Chronic pancreatitis is also characterized by the insufficient secretion of digestive enzymes from acinar cells, resulting in an impaired ability of the intestine to break down food. Resulting symptoms include a distended abdomen, weight loss, and diarrhea. The *Tfr1*$^{Panc\text{-}KO}$ mice which developed hyperglycemia exhibited all of these symptoms. Additionally, the large presence of fat in the stool, or steatorrhea, is another characteristic of chronic pancreatitis. Oil-red-O staining of wildtype and *Tfr1*$^{Panc\text{-}KO}$ stool detected the presence of excess fat in the form of large lipid droplets (white arrows) (**Figure 13**).

Islet histology and glucose homeostasis is unaffected after loss of Tfr1 in beta cells

Because the deletion of Tfr1 affects both the endocrine and exocrine tissue in *Tfr1*$^{Panc\text{-}KO}$ pancreas, it was difficult to determine whether the disruption of each tissue occurred independently or if disruption of one part occurred as a consequence of disruption of the other. To resolve this, we generated a β cell-specific conditional knockout (*Tfr1*$^{Beta\text{-}KO}$) mouse by crossing *Tfr1*$^{fl/fl}$ mice with rat *ins2-Cre* transgenic mice. The *ins2-Cre* transgene expresses Cre recombinase in β-cells as well as in the hypothalamus.

H&E staining of 2 month old wildtype and *Tfr1*$^{Beta\text{-}KO}$ pancreases show acinar cells which are normal in morphology as expected. Surprisingly, islets of Langerhans were detected in the *Tfr1*$^{Beta\text{-}KO}$ pancreas and appeared normal in both number and mass (**Figure 14**). This evidence suggests that the loss of Tfr1 specifically in β-cells does not have an effect on their development, growth, or upkeep. Further work is needed to validate Tfr1 deletion in β-cells.

Because hyperglycemia and destruction of islets is a progressive process, *Tfr1*$^{Beta\text{-}KO}$ mice were aged to a year and blood glucose levels were measured to determine whether the loss of Tfr1 in β-cells had an effect on glucose homeostasis in the long term. There was no significant difference in blood glucose levels between 1 year old wildtype and *Tfr1*$^{Beta\text{-}KO}$ mice (**Figure 15**), suggesting that β-cells are maintained in the *Tfr1*$^{Beta\text{-}KO}$ islets. Further work will assay the amount of *Tfr1* loss in β-cells.

3.4 Discussion

The loss of Tfr1 in *Tfr1*$^{Panc\text{-}KO}$ pancreas results in characteristics found in pancreatitis. The loss of islets and corresponding loss of β-cells observed in the *Tfr1*$^{Panc\text{-}KO}$ pancreas resulted in decreased serum insulin levels and subsequent hyperglycemia as seen in diabetes. There is evidence of abnormal collagen accumulation and steatorrhea, as observed in pancreatitis, suggested that the loss of Tfr1 causes some form of damage to the pancreas, leading to exocrine pancreatic insufficiency. The normal pancreatic histology and blood glucose levels found in the *Tfr1*$^{Beta\text{-}KO}$ mouse model, suggested that Tfr1 is not required for β-cell development or maintenance. Therefore, we infer that the loss of β-cells in the *Tfr1*$^{Panc\text{-}KO}$ pancreas was secondary to the disruption observed in the exocrine tissue, possibly due to damage to the islets caused by autodigestion by digestive enzymes. Autophagy can activate trypsinogen and cause pancreatic autodigestion in mouse models of acute pancreatitis. An increase in LC-3 was observed in the *Tfr1*$^{Panc\text{-}KO}$

pancreatic tissue (**Figure 16**), suggesting that enhanced autophagy might contribute to tissue damage. This damage could be caused by a requirement of Tfr1 for acinar cell survival or proper digestive enzyme secretion. Alternatively, it might be that ductal epithelial cells, lacking Tfr1, have abnormalities that impair the drainage of digestive enzymes from acinar clusters.

Future work will determine whether features of acute pancreatitis such as inflammation, neutrophilic infiltration, and necrosis contribute to the damage observed in the affected regions of the *Tfr1*$^{Panc\text{-}KO}$ pancreas. Further work is also needed to verify Tfr1 deletion in *Tfr1*$^{Panc\text{-}KO}$ pancreas and *Tfr1*$^{Beta\text{-}KO}$ beta cells at the mRNA and protein levels. Lastly, a transgenic mouse model expressing pancreatic trypsin inhibitor I in acinar cells has been shown to rescue caerulein-induced pancreatitis and this mouse model could be bred with *Tfr1*$^{Panc\text{-}KO}$ mice to determine whether inhibiting trypsin activity in the pancreatitis phenotype would rescue the diabetic phenotype.

Work has begun to determine whether Tfr1 has additional, non-canonical roles in the pancreas. We have observed some rescue of lethality or extension of viability in both *Tfr1*$^{Panc\text{-}KO}$;*Rosa26*^{Tfr1R654A} mice and in iron-dextran injected *Tfr1*$^{Panc\text{-}KO}$ mice, but the numbers of mice in each group were too small to be conclusive and more detailed characterization is needed.

In order to assay transcriptional changes in the pancreas of *Tfr1*$^{Panc\text{-}KO}$ mice, the ductal, acinar, and β-cell populations can be segregated by flow cytometric identification of cell surface markers specific to each population. These three populations can be sorted through flow cytometry and differential gene expression analysis using microarray RNA profiling can be used to compare wildtype and *Tfr1*$^{Panc\text{-}KO}$ cells to ascertain candidate genes affected by the loss of Tfr1.

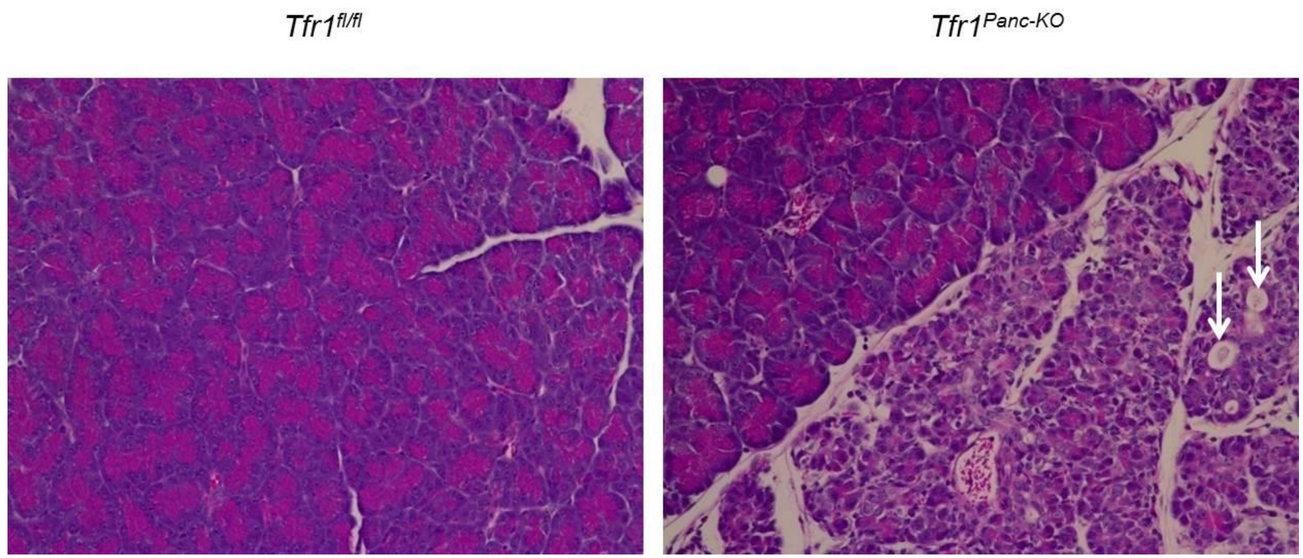
$Tfr1^{fl/fl}$
$Tfr1^{Panc\text{-}KO}$

Figure 8. Disrupted exocrine tissue and reduced islets in *Tfr1*$^{Panc\text{-}KO}$ pancreas.

H&E staining of sections prepared from 4 week old wildtype and *Tfr1*$^{Panc\text{-}KO}$ pancreases was used to evaluate gross pancreatic architecture. White arrows point to possible enlarged ducts.

Insulin

Insulin
Dapi

Tfr1$^{fl/fl}$

Tfr1$^{Panc\text{-}KO}$

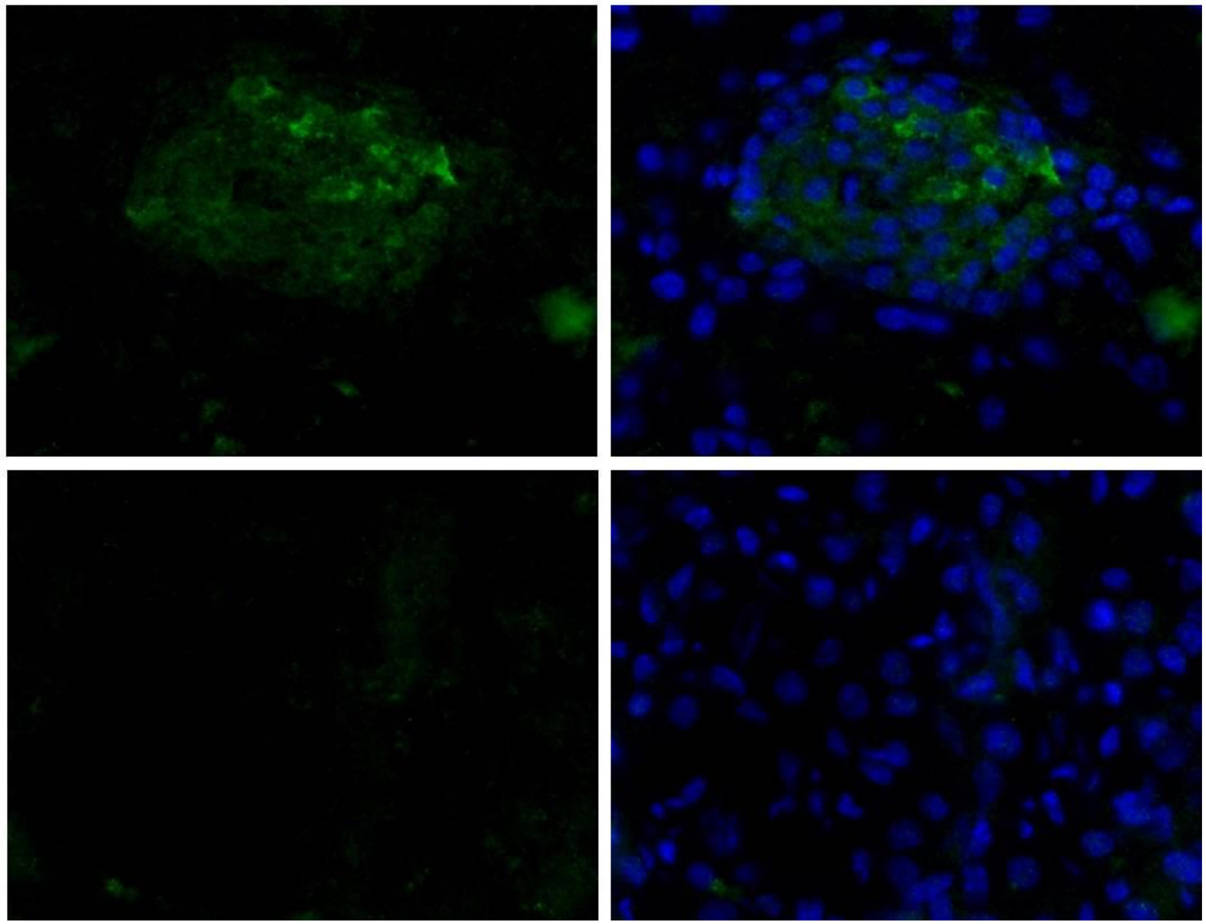

Figure 9. Fewer β-cells in *Tfr1*$^{Panc\text{-}KO}$ pancreas.

Sections of 4 week old wildtype and *Tfr1*$^{Panc\text{-}KO}$ pancreases were stained for insulin (green) and DAPI (blue) in order to show scarcity of β-cells.

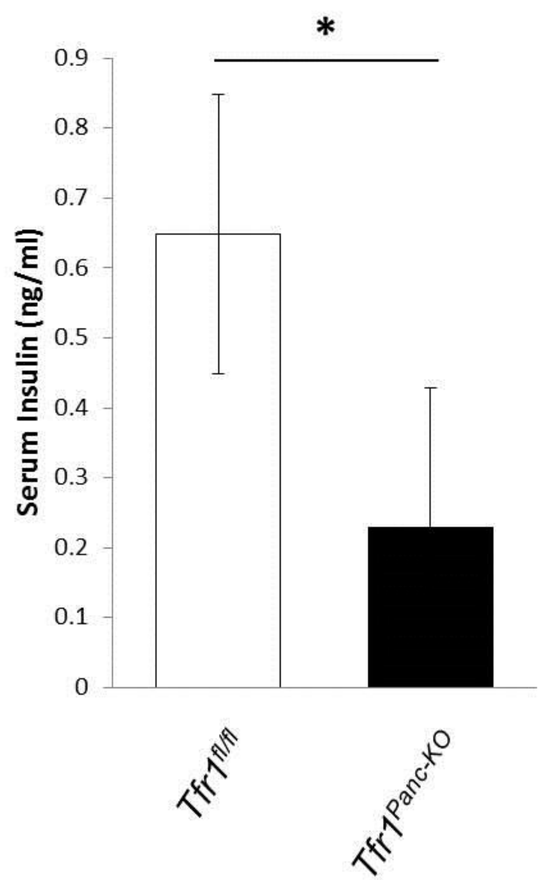
*
Serum Insulin (ng/ml)
0.9
0.8
0.7
0.6
0.5
0.4
0.3
0.2
0.1
0
Tfr1fl/fl
Tfr1Panc-KO

Figure 10. Reduced serum insulin levels in *Tfr1*$^{Panc\text{-}KO}$ mice

Serum insulin levels were measured in 4 week old wildtype (n=7) and *Tfr1*$^{Panc\text{-}KO}$ (n=7) mice ($p<0.05$).

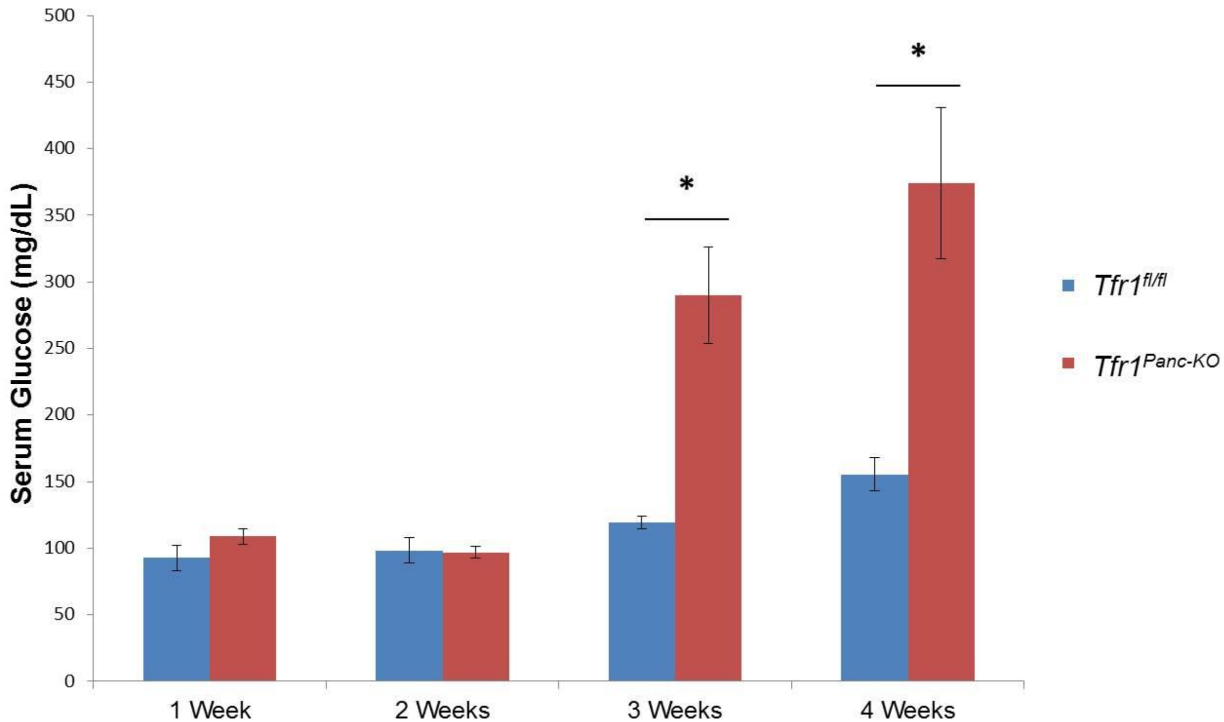
Serum Glucose (mg/dL)
500
450
400
350
300
250
200
150
100
50
0
*
*
1 Week
2 Weeks
3 Weeks
4 Weeks
Tfr1fl/fl
Tfr1Panc-KO

Figure 11. Development of hyperglycemia in *Tfr1*$^{Panc\text{-}KO}$ mice.

Blood glucose levels were measured from 1 week, 2 week, 3 week ($p<0.05$), and 4 week old ($p<0.05$) wildtype ($n=7$) and *Tfr1*$^{Panc\text{-}KO}$ ($n=9$) mice.

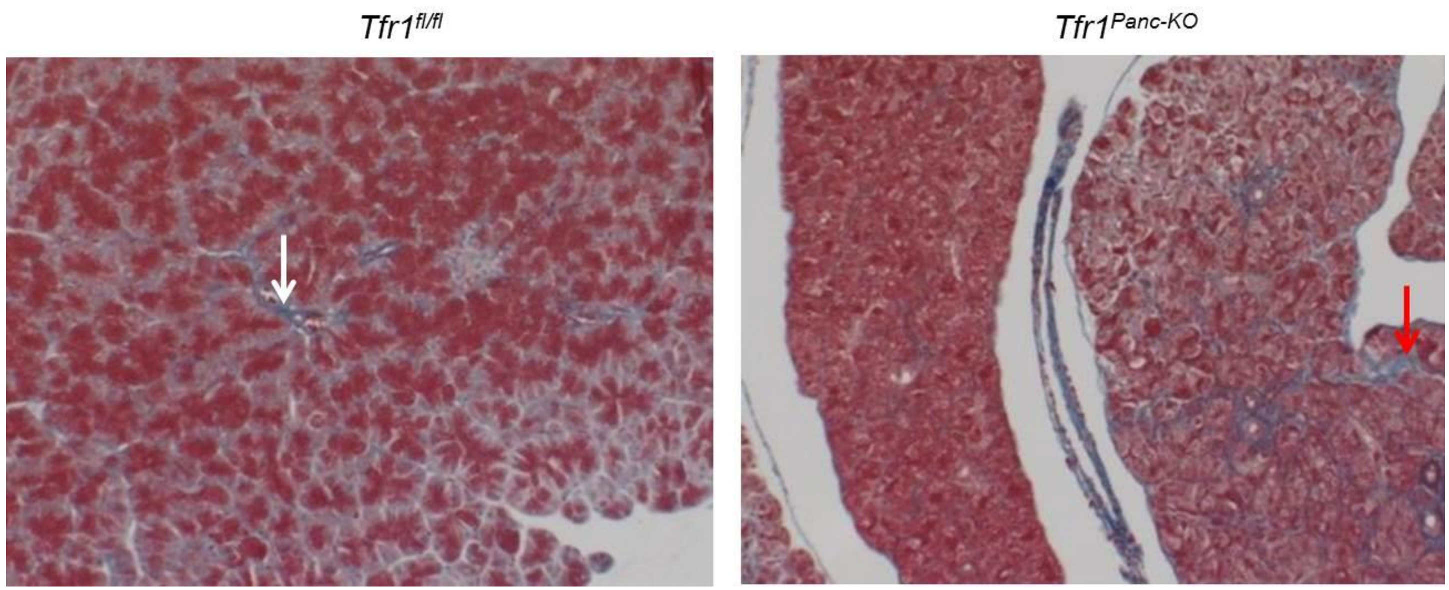
Tfr1fl/fl
Tfr1Panc-KO

Figure 12. Presence of mild fibrosis in *Tfr1*$^{Panc\text{-}KO}$ pancreas

Sections of 4 week old wildtype and *Tfr1*$^{Panc\text{-}KO}$ pancreases were stained for Masson's Trichrome to assess for the presence of collagen (blue). White arrow denotes collagen in wildtype blood vessels. Red arrow denotes collagen interspersed between acinar cells.

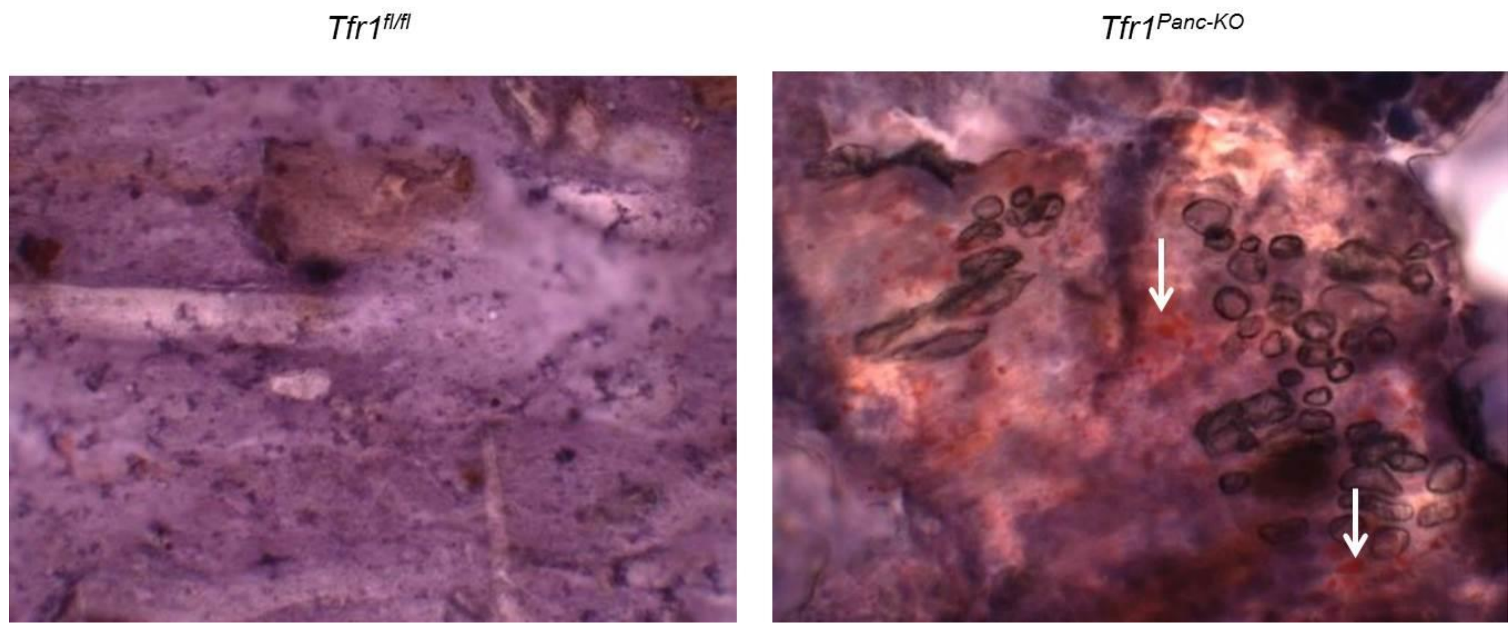

$Tfr1^{fl/fl}$
$Tfr1^{Panc\text{-}KO}$

Figure 13. ***Tfr1$^{Panc\text{-}KO}$*** **mice have steatorrhea.**

Fecal smears of 4 week old wildtype and *Tfr1$^{Panc\text{-}KO}$* were stained for Oil-red-O to assess for the presence of neutral lipids in the form of lipid droplets (white arrows) in the stool.

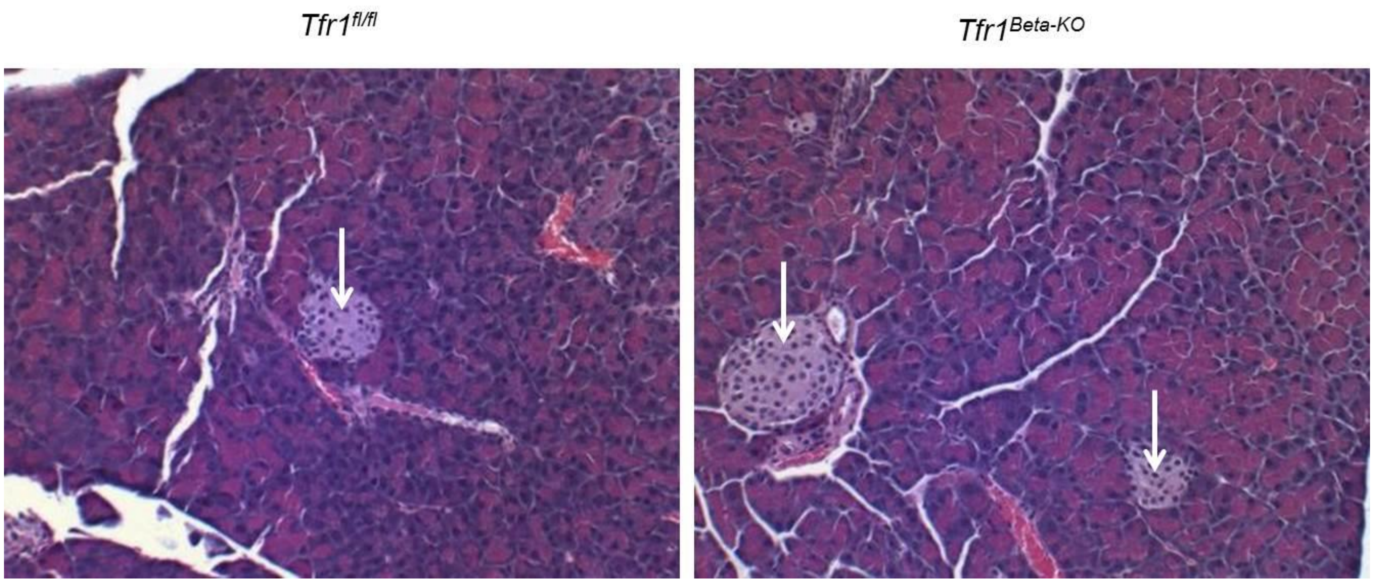
$Tfr1^{fl/fl}$
$Tfr1^{Beta\text{-}KO}$

Figure 14. Islets of Langerhans appear intact in *Tfr1*$^{Beta\text{-}KO}$ pancreas.

H&E staining of sections prepared from 2 month old wildtype and *Tfr1*$^{Beta\text{-}KO}$ pancreases was used to evaluate gross pancreatic architecture. Islets (white arrow) were present in *Tfr1*$^{Beta\text{-}KO}$ pancreas.

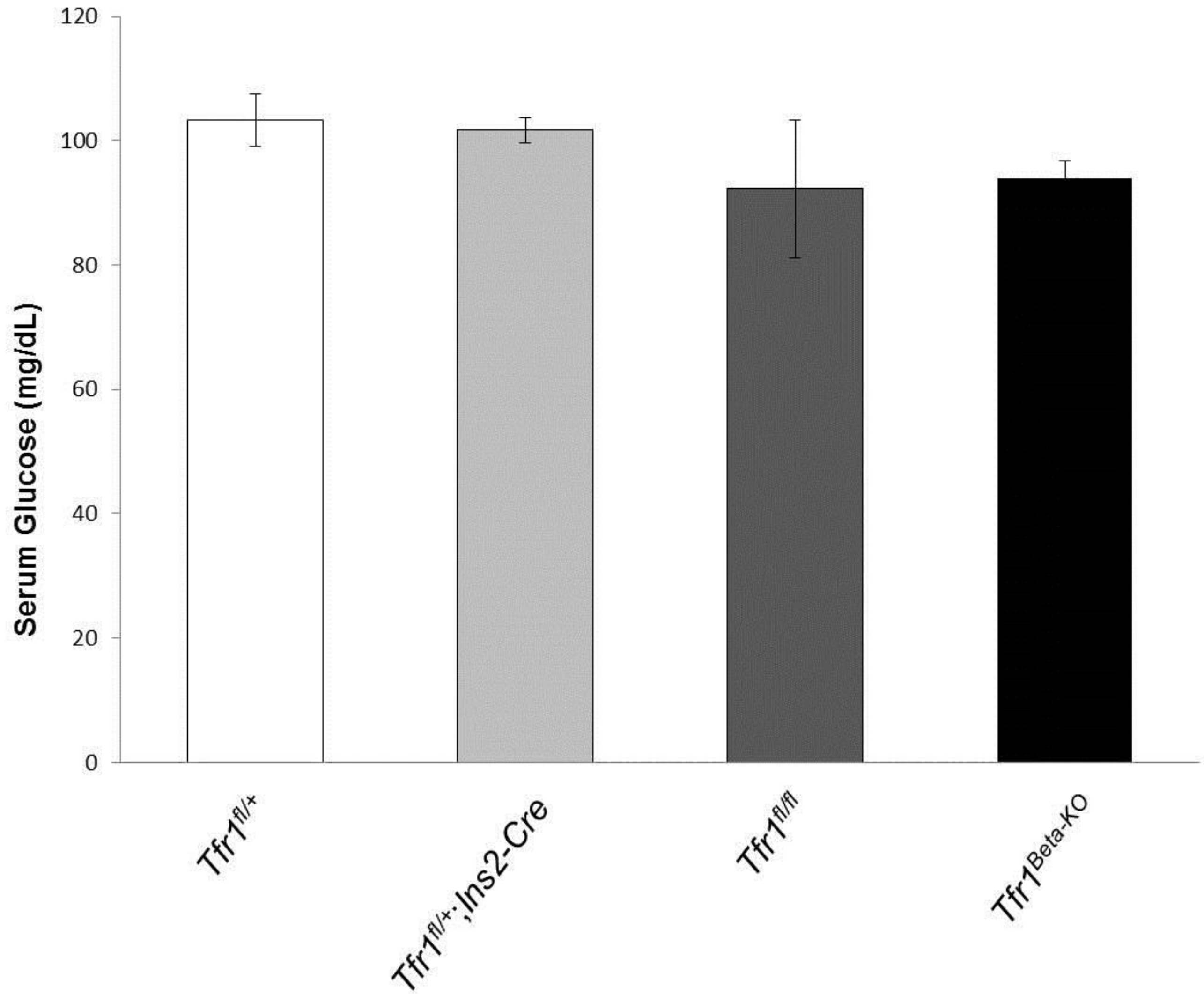
Serum Glucose (mg/dL)
0
20
40
60
80
100
120
Tfr1fl/+
Tfr1fl/+;Ins2-Cre
Tfr1fl/fl
Tfr1Beta-KO

Figure 15. ***Tfr1**$^{Beta\text{-}KO}$* **mice have normal serum glucose levels.**

Blood glucose levels were measured from 1 year old *Tfr1*$^{fl/+}$ (n=6), *Tfr1*$^{fl/+}$;*Ins2-Cre* (n=6), wildtype (n=6) and *Tfr1*$^{Beta\text{-}KO}$ (n=6) mice.

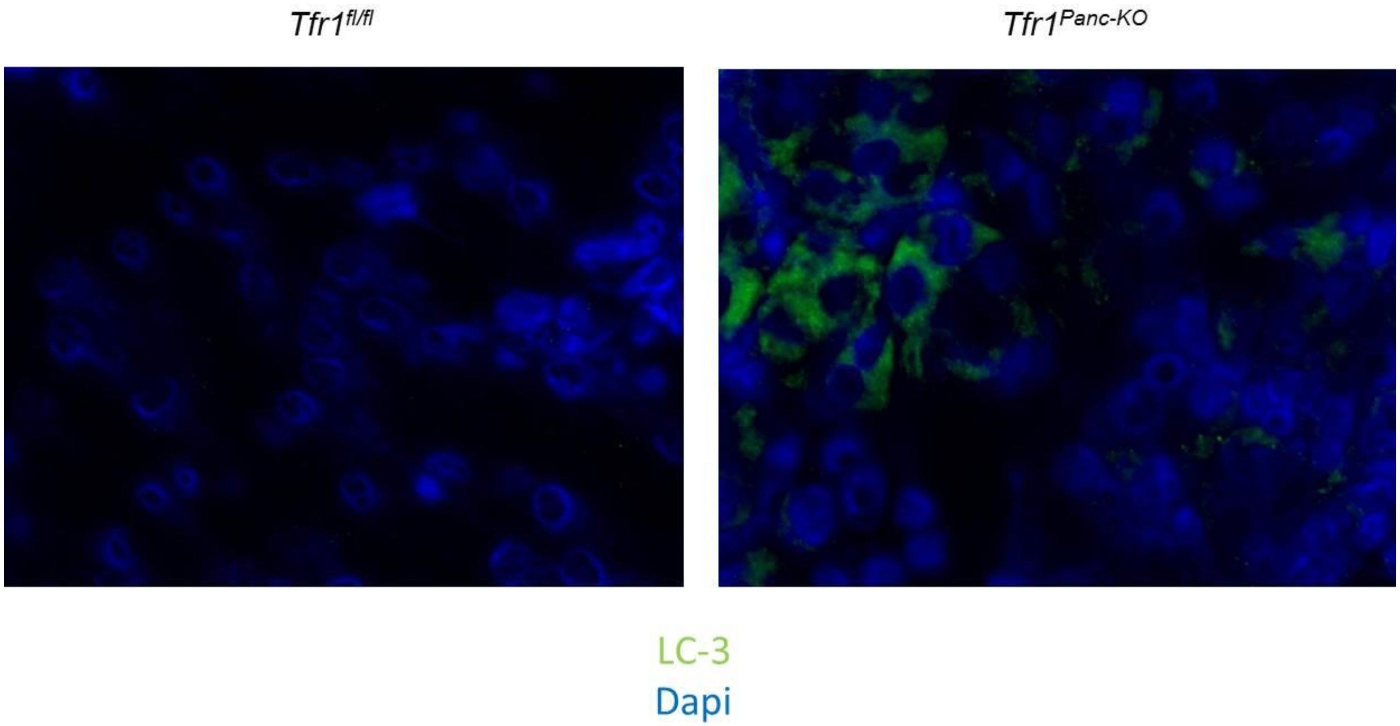

Tfr1fl/fl
Tfr1Panc-KO
LC-3
Dapi

Figure 16. *Tfr1*$^{Beta\text{-}KO}$ mice have increased autophagy.

Immunofluorescence was performed for LC-3 (green) and DAPI (blue) in order to assess autophagy in wildtype and *Tfr1*$^{Beta\text{-}KO}$ mice.

4. The transferrin receptor in the skin

4.1 Introduction

Like the intestinal epithelium, the skin is a tissue which undergoes constant proliferation in order to maintain homeostasis to serve as a protective barrier against the environment and minimize bodily water loss. The skin contains a stratified epithelium consisting of the interfollicular epidermis and hair follicles. The basal layer of the interfollicular epidermis contains epidermal stem cells and transit amplifying cells, which proliferate and differentiate into mature keratinocytes. During the process of differentiation, keratinocytes move upward and are sloughed off after they have reached the stratum corneum, the outermost layer of the epidermis (*49*). Hair follicle stem cells reside in the bulge of hair follicles and give rise to transit amplifying cells which line the outer root sheath. The transit amplifying cells of the outer root sheath contribute to matrix cells lining the bottom of the hair follicle, which differentiate into the hair channel, the inner root sheath, and the hair strand (*50*).

Expression of Tfr1 in the skin epidermis is tightly linked with the proliferative capacity of the resident cell type. High levels of Tfr1 are found in transit amplifying cells while low levels of Tfr1 are found in stem cells, as shown through flow cytometry and label retaining experiments (*51*). In accordance with these results, Tfr1 immunofluorescence experiments have shown the brightest Tfr1 staining in the basal interfollicular epidermis and in the matrix of the hair follicle, while dim Tfr1 staining was observed in the follicular bulge region (*52,53*).

The skin epidermis is a tissue associated with iron uptake and storage. An increase in iron levels in the epidermis was observed in mouse models of dietary iron overload and parenteral iron injections (*54*). Desquamation of keratinocytes is a major route of iron loss in counterbalancing dietary iron uptake (*55*). Tfr1 is associated with iron acquisition in the skin epidermis. A transgenic mouse model in which Tfr1 expression was enforced by the epidermal-specific *keratin 14* promoter showed elevated levels of iron in the dorsal skin epithelium (*56*). However, whether Tfr1 plays an important physiological role in iron uptake in the skin epithelium or if it possesses any additional roles is still unknown.

4.2 Materials and Methods

Mouse breeding

$Tfr1^{Skin\text{-}KO}$ mice were generated by crossing $Tfr1^{fl/fl}$ mice with *K14-Cre* mice. Resulting progeny were intercrossed to generate $Tfr1^{fl/+}$; *K14-Cre* mice in the F2 generation, which were used as parents to produce the F3 generation used in experiments. Wildtype controls for both mouse strains were $Tfr1^{fl/fl}$ or $Tfr1^{fl/+}$,which have no phenotype.

Immunohistochemistry

A small square of dorsal skin epithelium was dissected from P5 pups and fixed overnight in 10% formalin followed by 70% ethanol. Skin pieces were embedded vertically in paraffin and sectioned longitudinally. Hematoxylin and eosin staining was performed after sections were deparaffinized and rehydrated. Ki67 staining was performed was performed after antibody retrieval by boiling the slide in 10mM sodium citrate buffer pH 6.0.

Immunofluorescence

A small square of dorsal skin epithelium was dissected from P5 pups, embedded in OCT media, and snap frozen in liquid nitrogen. Skin pieces were then sectioned longitudinally, fixed with ice cold acetone for 15 minutes, and permeabilized with 0.1% Tween-20. Sections were stained with rabbit anti-keratin 6 antibody (Covance), goat anti-rabbit Alexafluor 488 secondary (Life Technologies), and DAPI.

Terminal Deoxynucleotidyl Transferase dUTP Nick End Labeling (TUNEL) Apoptosis Assay

Paraffin embedded skin sections were deparaffinized, rehydrated, and permeabilized with 0.1% Triton-100. TUNEL-FITC staining was performed using the Fluorescein *in situ* Cell Detection Kit (Roche).

4.3 Results

Neonatal lethality in mice with conditional deletion of *Tfr1* in the skin epidermis

We generated a skin-epidermis specific conditional knockout ($Tfr1^{Skin\text{-}KO}$) mouse model by crossing $Tfr1^{fl/fl}$ mice with human *keratin 14-Cre* transgenic mice. Keratin 14, a component intermediate fiber found in epithelial cells, is expressed in the basal interfollicular skin epidermis as well as in the outer root sheaths of hair follicles (*57*). *Keratin 14-Cre* transgene expression was detected in the skin and dental epithelium by E14.5 (*58*).

Tfr1$^{Skin\text{-}KO}$ mice were born in Mendelian ratios and were indistinguishable from their wildtype littermates at birth. Starting at P4, the *Tfr1*$^{Skin\text{-}KO}$ pups fail to thrive (**Figure 17**), resulting in their deaths between P7 to P9. Penetrance of the lethal phenotype was 96% in our experiments with a lone *Tfr1*$^{Skin\text{-}KO}$ female mouse surviving into adulthood, possibly due to low recombination efficiency. The escaper mouse showed no overt signs of skin defects and was of normal body weight compared with wildtype littermates. As keratin 14 is also expressed in the oral ectoderm during development (*59*), the mouth was examined for any defects. Lack of any gross abnormalities in the mouth and tongue of the *Tfr1*$^{Skin\text{-}KO}$ pups as well as the presence of milk in the stomach suggests that deletion of Tfr1 in the skin epidermis may be the main cause of the neonatal lethality.

Gross epidermal architecture of skin appears unaffected in *Tfr1*$^{Skin\text{-}KO}$ mice

In order to assess the general architecture of the skin epithelium, hematoxylin and eosin (H&E) and Ki67 was performed on the dorsal skin epithelium of P5 wildtype and *Tfr1*$^{Skin\text{-}KO}$ mice. H&E staining showed no breakage of the stratum corneum much like the wildtype (**Figure 18**). Hair follicles were present in *Tfr1*$^{Skin\text{-}KO}$ mouse, however, the morphology of the hair follicles appeared abnormal. Most strikingly, a severe loss of adipocytes was observed in *Tfr1*$^{Skin\text{-}KO}$ mice at P5. Ki67 staining showed no loss of proliferating cells in the basal layer of the interfollicular *Tfr1*$^{Skin\text{-}KO}$ skin (**Figure 18**). However, proliferation within the root sheaths of the hair follicles appeared abnormal.

Wound healing is a property of skin epidermis which is initiated after barrier function has been compromised. Wound healing is characterized by the induction of keratin 6 at the wound edge ahead of the migration of epithelial cells into the wound site (*60*). To determine if the loss of Tfr1 in the skin caused a phenotype similar to wound healing, P5 dorsal skin epithelia of *Tfr1*$^{Skin\text{-}KO}$ and wildtype pups were stained for keratin 6. Immunofluorescence for keratin 6 showed less staining in *Tfr1*$^{Skin\text{-}KO}$ skin compared to wildtype, preliminarily suggesting that the loss of Tfr1 does not induce the wound healing response (**Figure 19**).

Increased apoptosis in the skin epidermis of *Tfr1*$^{Skin\text{-}KO}$ mice

Loss of Tfr1 in cardiomyocytes resulted in increased apoptosis (Wenjing Xu, unpublished data). In order to assess whether the loss of Tfr1 in the skin epithelium shows a similar increase in apoptosis, TUNEL staining was performed in P5 dorsal skin epithelia of *Tfr1*$^{Skin\text{-}KO}$ and wildtype pups. *Tfr1*$^{Skin\text{-}KO}$ skin showed a marked increase in apoptosis in both the basal epithelium (white arrow) as well as within the root sheaths of hair follicles (red arrow) (**Figure 20**). Interestingly, increased apoptosis was also observed in a population of cells interspersed between hair follicles (yellow arrow), possibly corresponding to intradermal adipocytes.

4.4 Discussion

Given the phenotype of the *Tfr1*$^{IEC\text{-}KO}$ pups and the similarity in developmental hierarchy between intestinal and skin epithelial cells, initial efforts in characterizing the *Tfr1*$^{Skin\text{-}KO}$ pups were focused on determining the effects of the loss of Tfr1 on skin epithelial barrier function and proliferation. Gross epidermal architecture appeared uncompromised as assessed through H&E staining. No signs of bleeding or infection were observed in regions of the skin subjected to high mechanical stress, such as between digits. Furthermore, wound healing response, a sign of compromised barrier function, did not appear to be initiated as the levels of keratin 6 was not elevated in the *Tfr1*$^{Skin\text{-}KO}$ skin. It is possible that the increase in apoptotic cells observed in the *Tfr1*$^{Skin\text{-}KO}$ is an intrinsic response to the loss of Tfr1 rather than a secondary response due to a barrier defect. The number of proliferative cells in the basal epidermis appears unaffected by the increase in apoptosis, possibly due to an increase in proliferation as a compensatory measure. However, more work is needed to fully quantify levels of proliferation.

Future work will focus on characterizing the levels of Tfr1 at the mRNA and protein levels in primary keratinocytes isolated from wildtype and *Tfr1*$^{Skin\text{-}KO}$ pups. Because of the existence of the escaper *Tfr1*$^{Skin\text{-}KO}$ mouse, it will be critical to determine the levels of residual Tfr1 in *Tfr1*$^{Skin\text{-}KO}$ mice. H&E, Ki67, and TUNEL staining of the skin epithelium, coupled with RT-PCR of primary keratinocytes, at earlier time points will be essential to determine when the phenotype manifests itself and to correlate transcriptional changes after the loss of Tfr1 to early or late timepoints. The primary cause of the neonatal lethality will also be the focus of future work. Hypothermia due to impaired adipose development could be a possibility.

Tfr1 has been shown to have iron-independent roles in the intestinal epithelium. To determine if this is the case in the skin, *Tfr1*$^{Skin\text{-}KO}$;*Rosa26*^{Tfr1R654A} mice will be generated and *Tfr1*$^{Skin\text{-}KO}$ pups will be injected with iron-dextran in order to observe any extension of viability or rescue of lethality.

Finally, the striking loss of adipocytes seen in the *Tfr1*$^{Skin\text{-}KO}$ will be the focus of future work. A correlation between the growth of the hair follicle and adipocyte development has been observed in mice. During the anagen phase of hair follicle growth, the dermal adipocyte layer increases in thickness (*61*). Conversely, during the telogen phase of hair follicle growth, the adipose layer becomes thinner. In wildtype neonates, hair follicles undergo the anagen phase up to P15 with a corresponding thickening to the dermal adipose layer. The abnormal phenotype and increased apoptosis of the *Tfr1*$^{Skin\text{-}KO}$ hair follicle coupled with the inability of the adipose layer to thicken during development suggests an impairment in this process. One possible candidate pathway that might explain this impairment in the relationship between hair follicle development and adipose thickening is Wnt signaling. The loss of Wnt signaling in the epidermis delays the ability of the hair follicle to undergo the anagen phase, while activation of Wnt signaling induces hair follicles to enter the anagen phase in mice (*62*). Furthermore, activation of Wnt signaling in the skin epidermis induces secretion of ligands which promotes adipocyte differentiation (*63*). The *Tfr1*$^{Skin\text{-}KO}$ mouse model will be useful in determining the relationship between Tfr1, Wnt signaling, and the interdependence of hair follicle growth with adipose development.


Tfr1fl/fl
Tfr1Skin-KO

Figure 17. ***Tfr1*$^{Skin\text{-}KO}$ pups at fail to thrive**.

Body sizes of wildtype and *Tfr1*$^{Skin\text{-}KO}$ pups at P5.

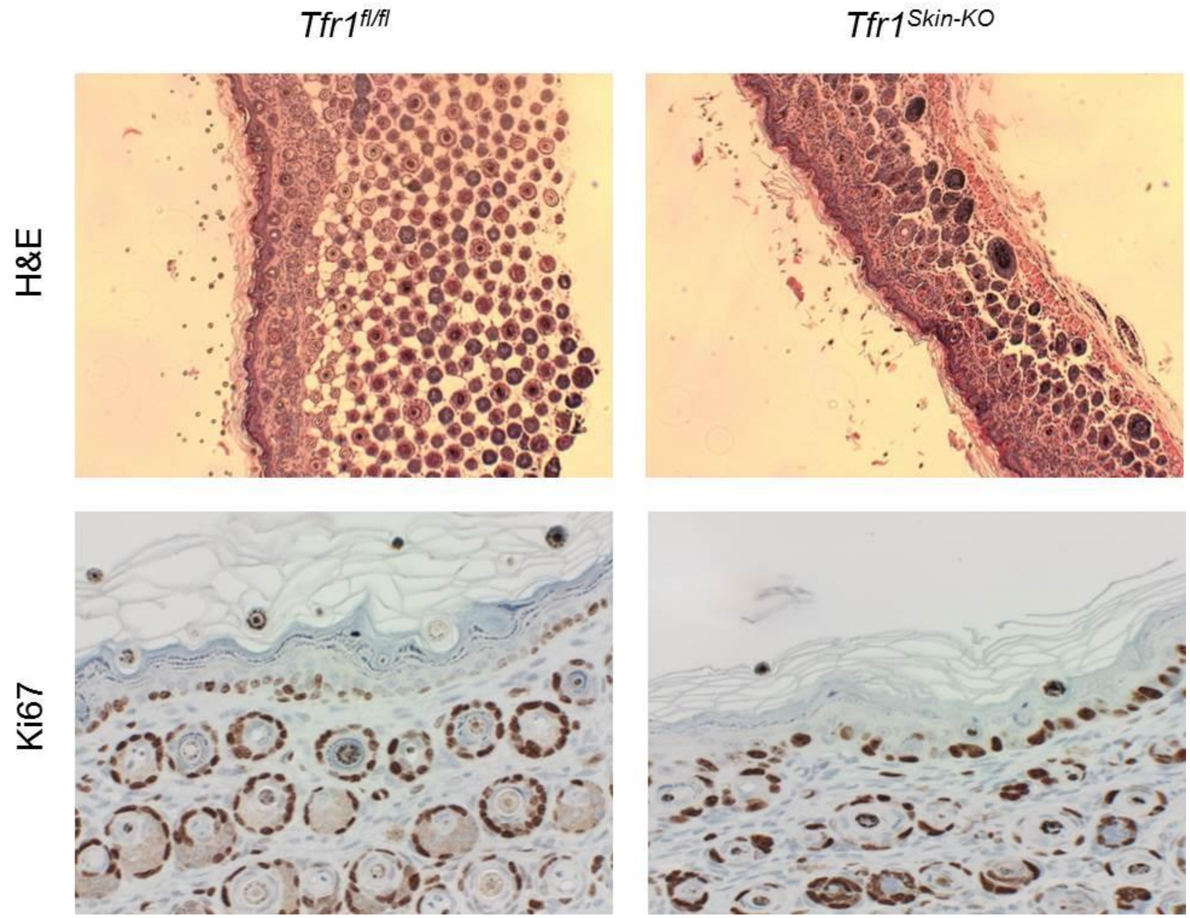
Tfr1fl/fl
Tfr1Skin-KO
H&E
Ki67

Figure 18. Gross architecture remains intact in *Tfr1*$^{Skin\text{-}KO}$ skin epithelium, but lack of adipose layer and abnormal proliferation is observed in root sheaths.

Sections of wildtype and *Tfr1*$^{Skin\text{-}KO}$ dorsal skin at P5 were stained with H&E or Ki67 to evaluate overall architecture and proliferation, respectively. The architecture of *Tfr1*$^{Skin\text{-}KO}$ dorsal skin is abnormal, with a prominent deficiency of adipose tissue. Overall, proliferation appeared to be similar in wildtype and mutant animals.

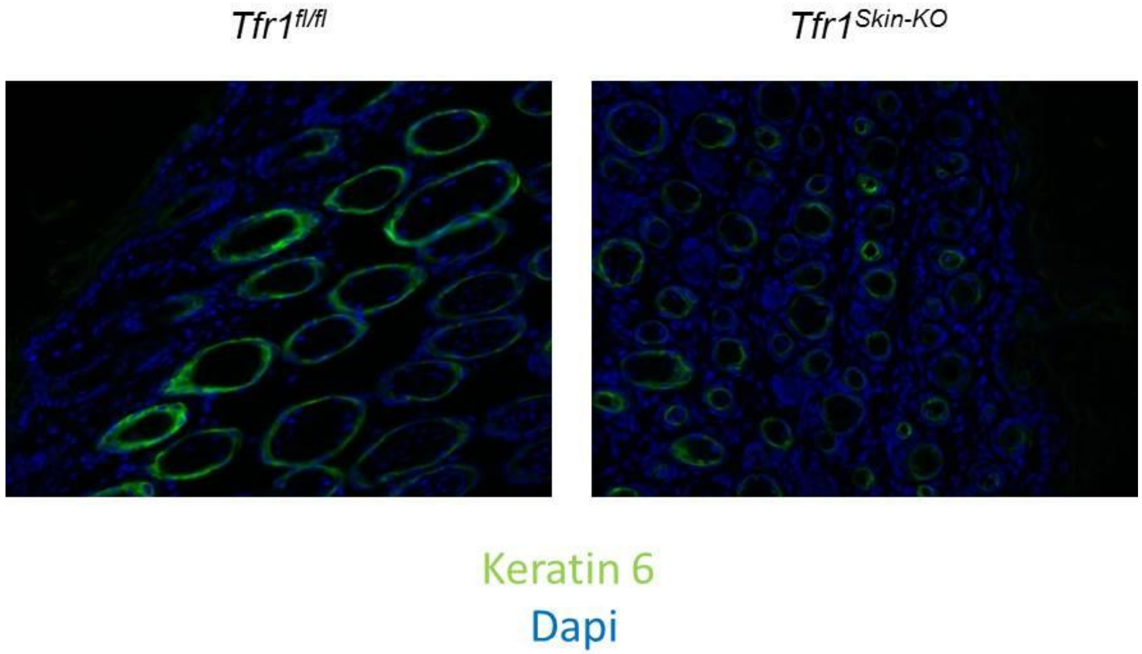

Tfr1$^{fl/fl}$
Tfr1$^{Skin\text{-}KO}$
Keratin 6
Dapi

Figure 19. Levels of keratin 6 are not elevated in *Tfr1*$^{Skin\text{-}KO}$ skin epithelium.

Sections of wildtype and *Tfr1*$^{Skin\text{-}KO}$ dorsal skin at P5 were stained for Keratin 6 (green) and DAPI (blue).

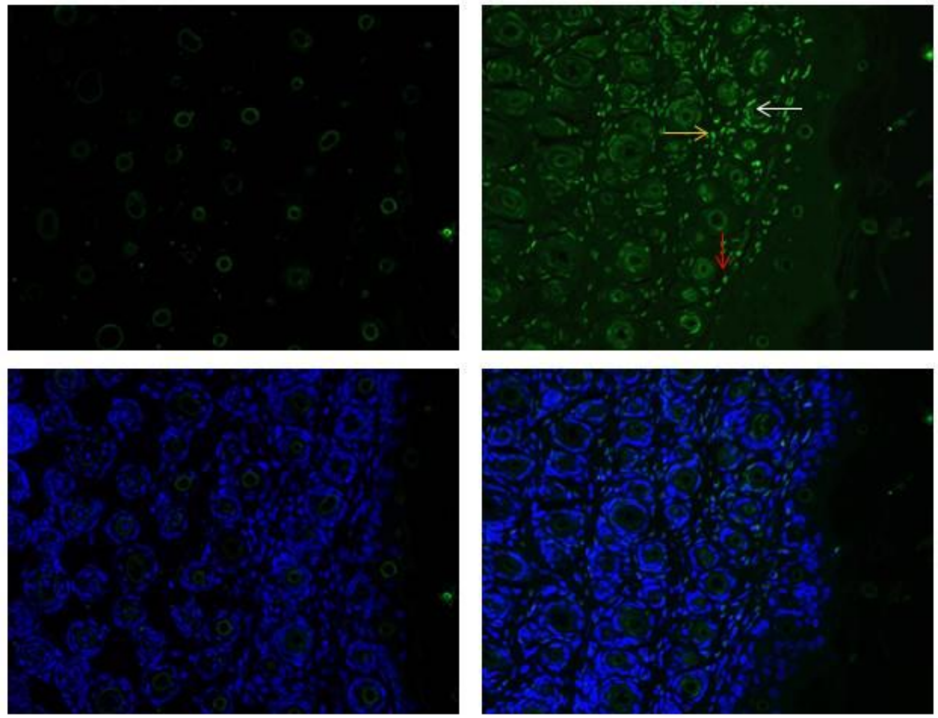

Red arrow – basal epidermis
Yellow arrow – interfollicular region
White arrow – hair follicle

Figure 20. Increase in apoptosis in *Tfr1*$^{Skin\text{-}KO}$ skin epithelium at P5.

Sections of wildtype and *Tfr1*$^{Skin\text{-}KO}$ dorsal skin at P5 were stained with Tunel-FITC (green) and DAPI (blue). Dual FITC and DAPI positive cells are seen in the basal epidermal layer (white arrow), root sheath (red arrow), and interfollicular region (yellow arrow

References

1. Moura IC, Hermine O, Lacombe C, Mayeux P. Erythropoiesis and transferrin receptors. Curr Opin Hematol. 2015 Mar 12.

2. Levy JE, Jin O, Fujiwara Y, Kuo F, Andrews NC. Transferrin receptor is necessary for development of erythrocytes and the nervous system. Nat Genet. 1999;21:396–9.

3. Zhu BM, McLaughlin SK, Na R, Liu J, Cui Y, Martin C, Kimura A, Robinson GW, Andrews NC, Hennighausen L. Hematopoietic-specific Stat5-null mice display microcytic hypochromic anemia associated with reduced transferrin receptor gene expression. Blood. 2008 Sep 1;112(5):2071-80.

4. http://biogps.org/#goto=genereport&id=22042

5. Ned, R.M., Swat, W., and Andrews, N.C. (2003). Transferrin receptor 1 is differentially required in lymphocyte development. Blood *102*, 3711-3718.

6. Trenor, C.C., 3rd, Campagna, D.R., Sellers, V.M., Andrews, N.C., and Fleming, M.D. (2000). The molecular defect in hypotransferrinemic mice. Blood *96*, 1113-1118.

7. Schmidt, P.J., Toran, P.T., Giannetti, A.M., Bjorkman, P.J., and Andrews, N.C. (2008). The transferrin receptor modulates Hfe-dependent regulation of hepcidin expression. Cell Metab *7*, 205-214.

8. Matysiak-Budnik, T., Moura, I.C., Arcos-Fajardo, M., Lebreton, C., Menard, S., Candalh, C., Ben-Khalifa, K., Dugave, C., Tamouza, H., van Niel, G., *et al.* (2008). Secretory IgA mediates retrotranscytosis of intact gliadin peptides via the transferrin receptor in celiac disease. J Exp Med *205*, 143-154.

9. Radoshitzky, S.R., Abraham, J., Spiropoulou, C.F., Kuhn, J.H., Nguyen, D., Li, W., Nagel, J., Schmidt, P.J., Nunberg, J.H., Andrews, N.C., *et al.* (2007). Transferrin receptor 1 is a cellular receptor for New World haemorrhagic fever arenaviruses. Nature *446*, 92-96.

10. Allison, A.B., Kohler, D.J., Ortega, A., Hoover, E.A., Grove, D.M., Holmes, E.C., and Parrish, C.R. (2014). Host-specific parvovirus evolution in nature is recapitulated by in vitro adaptation to different carnivore species. PLoS Pathog *10*, e1004475.

11. Worthen, C.A., and Enns, C.A. (2014). The role of hepatic transferrin receptor 2 in the regulation of iron homeostasis in the body. Frontiers in pharmacology *5*, 34.

12. Pinto, J.T., Suffoletto, B.P., Berzin, T.M., Qiao, C.H., Lin, S., Tong, W.P., May, F., Mukherjee, B., and Heston, W.D. (1996). Prostate-specific membrane antigen: a novel folate hydrolase in human prostatic carcinoma cells. Clin Cancer Res *2*, 1445-1451.

13. Lambert, L.A., and Mitchell, S.L. (2007). Molecular evolution of the transferrin receptor/glutamate carboxypeptidase II family. Journal of molecular evolution *64*, 113-128.

14. Batista, A., Millan, J., Mittelbrunn, M., Sanchez-Madrid, F., and Alonso, M.A. (2004). Recruitment of transferrin receptor to immunological synapse in response to TCR engagement. J Immunol *172*, 6709-6714.

15. Salmeron, A., Borroto, A., Fresno, M., Crumpton, M.J., Ley, S.C., and Alarcon, B. (1995). Transferrin receptor induces tyrosine phosphorylation in T cells and is physically associated with the TCR zeta-chain. J Immunol *154*, 1675-1683.

16. Collawn, J.F., Lai, A., Domingo, D., Fitch, M., Hatton, S., and Trowbridge, I.S. (1993). YTRF is the conserved internalization signal of the transferrin receptor, and a second YTRF signal at position 30-34 enhances endocytosis. Journal of Biological Chemistry *268*, 21686-21692.

17. Cao, H., Chen, J., Krueger, E.W., and McNiven, M.A. SRC-mediated phosphorylation of dynamin and cortactin regulates the "constitutive" endocytosis of transferrin. Mol Cell Biol *30*, 781-792.

18. Ferrando, I.M., Chaerkady, R., Zhong, J., Molina, H., Jacob, H.K., Herbst-Robinson, K., Dancy, B.M., Katju, V., Bose, R., Zhang, J., *et al.* (2012). Identification of targets of c-Src tyrosine kinase by chemical complementation and phosphoproteomics. Mol Cell Proteomics *11*, 355-369.

19. Green, F., O'Hare, T., Blackwell, A., and Enns, C.A. (2002). Association of human transferrin receptor with GABARAP. FEBS Lett *518*, 101-106.

20. Ma, P., Schwarten, M., Schneider, L., Boeske, A., Henke, N., Lisak, D., Weber, S., Mohrluder, J., Stoldt, M., Strodel, B., *et al.* (2013). Interaction of Bcl-2 with the autophagy-related GABAA receptor-associated protein (GABARAP): biophysical characterization and functional implications. J Biol Chem *288*, 37204-37215.

21. Geminard, C., De Gassart, A., Blanc, L., and Vidal, M. (2004). Degradation of AP2 during reticulocyte maturation enhances binding of hsc70 and Alix to a common site on TFR for sorting into exosomes. Traffic *5*, 181-193.

22. Levine, D.S., and Woods, J.W. (1990). Immunolocalization of transferrin and transferrin receptor in mouse small intestinal absorptive cells. J Histochem Cytochem *38*, 851-858.

23. Clevers, H. (2013). The intestinal crypt, a prototype stem cell compartment. Cell *154*, 274-284.

24. Anderson GJ, Powell LW, Halliday JW. Transferrin receptor distribution and regulation in the rat small intestine. Effect of iron stores and erythropoiesis. Gastroenterology. 1990 Mar;98(3):576-85.

25. el Marjou, F., Janssen, K.P., Chang, B.H., Li, M., Hindie, V., Chan, L., Louvard, D., Chambon, P., Metzger, D., and Robine, S. (2004). Tissue-specific and inducible Cre-mediated recombination in the gut epithelium. Genesis *39*, 186-193.

26. Schmidt, P.J., Toran, P.T., Giannetti, A.M., Bjorkman, P.J., and Andrews, N.C. (2008). The transferrin receptor modulates Hfe-dependent regulation of hepcidin expression. Cell Metab *7*, 205-214.

27. Mootha, V.K., Lindgren, C.M., Eriksson, K.F., Subramanian, A., Sihag, S., Lehar, J., Puigserver, P., Carlsson, E., Ridderstrale, M., Laurila, E., *et al.* (2003). PGC-1alpha-responsive genes involved in oxidative phosphorylation are coordinately downregulated in human diabetes. Nat Genet *34*, 267-273.

28. Subramanian, A., Tamayo, P., Mootha, V.K., Mukherjee, S., Ebert, B.L., Gillette, M.A., Paulovich, A., Pomeroy, S.L., Golub, T.R., Lander, E.S., *et al.* (2005). Gene set enrichment analysis: a knowledge-based approach for interpreting genome-wide expression profiles. Proc Natl Acad Sci U S A *102*, 15545-15550.

29. Lamouille, S., Xu, J., and Derynck, R. (2014). Molecular mechanisms of epithelial-mesenchymal transition. Nat Rev Mol Cell Biol *15*, 178-196.

30. Mansbach, C.M., 2nd, and Gorelick, F. (2007). Development and physiological regulation of intestinal lipid absorption. II. Dietary lipid absorption, complex lipid synthesis, and the intracellular packaging and secretion of chylomicrons. Am J Physiol Gastrointest Liver Physiol *293*, G645-650.

31. Van Dyck, F., Braem, C.V., Chen, Z., Declercq, J., Deckers, R., Kim, B.M., Ito, S., Wu, M.K., Cohen, D.E., Dewerchin, M., *et al.* (2007). Loss of the PlagL2 transcription factor affects lacteal uptake of chylomicrons. Cell Metab *6*, 406-413.

32. Clevers, H. (2013). The intestinal crypt, a prototype stem cell compartment. Cell *154*, 274-284.

33. Xu, X., Li, W., Fan, X., Liang, Y., Zhao, M., Zhang, J., Liang, Y., Tong, W., Wang, J., Yang, W., *et al.* (2007). Identification and characterization of a novel p42.3 gene as tumor-specific and mitosis phase-dependent expression in gastric cancer. Oncogene *26*, 7371-7379.

34. Weng, Y.R., Yu, Y.N., Ren, L.L., Cui, Y., Lu, Y.Y., Chen, H.Y., Ma, X., Qin, W.X., Cao, W., Hong, J., *et al.* (2014). Role of C9orf140 in the promotion of colorectal cancer progression and mechanisms of its upregulation via activation of STAT5, beta-catenin and EZH2. Carcinogenesis *35*, 1389-1398.

35. Yuan, X.S., Zhang, Y., Guan, X.Y., Dong, B., Zhao, M., Mao, L.L., Lu, Y.Y., Tian, X.Y., and Hao, C.Y. (2013). p42.3: a promising biomarker for the progression and prognosis of human colorectal cancer. Journal of cancer research and clinical oncology *139*, 1211-1220.

36. Legesse-Miller, A., Elemento, O., Pfau, S.J., Forman, J.J., Tavazoie, S., and Coller, H.A. (2009). let-7 Overexpression leads to an increased fraction of cells in G2/M, direct down-regulation of Cdc34, and stabilization of Wee1 kinase in primary fibroblasts. J Biol Chem *284*, 6605-6609.

37. Cheung, T.H., Quach, N.L., Charville, G.W., Liu, L., Park, L., Edalati, A., Yoo, B., Hoang, P., and Rando, T.A. (2012). Maintenance of muscle stem-cell quiescence by microRNA-489. Nature *482*, 524-528.

38. Guo, S., Lu, J., Schlanger, R., Zhang, H., Wang, J.Y., Fox, M.C., Purton, L.E., Fleming, H.H., Cobb, B., Merkenschlager, M., *et al.* (2010). MicroRNA miR-125a controls hematopoietic stem cell number. Proc Natl Acad Sci U S A *107*, 14229-14234.

39. Liu, Z., Liu, H., Desai, S., Schmitt, D.C., Zhou, M., Khong, H.T., Klos, K.S., McClellan, S., Fodstad, O., and Tan, M. (2013). miR-125b functions as a key mediator for snail-induced stem cell propagation and chemoresistance. J Biol Chem *288*, 4334-4345.

40. Zheng, H., Ying, H., Wiedemeyer, R., Yan, H., Quayle, S.N., Ivanova, E.V., Paik, J.H., Zhang, H., Xiao, Y., Perry, S.R., *et al.* (2010). PLAGL2 regulates Wnt signaling to impede differentiation in neural stem cells and gliomas. Cancer Cell *17*, 497-509.

41. Kasibhatla, S., Jessen, K.A., Maliartchouk, S., Wang, J.Y., English, N.M., Drewe, J., Qiu, L., Archer, S.P., Ponce, A.E., Sirisoma, N., *et al.* (2005). A role for transferrin receptor in triggering apoptosis when targeted with gambogic acid. Proc Natl Acad Sci U S A *102*, 12095-12100.

42. Jian, J., Yang, Q., and Huang, X. (2011). Src regulates Tyr(20) phosphorylation of transferrin receptor-1 and potentiates breast cancer cell survival. J Biol Chem *286*, 35708-35715.

43. Prasad, S., Pandey, M.K., Yadav, V.R., and Aggarwal, B.B. (2011). Gambogic acid inhibits STAT3 phosphorylation through activation of protein tyrosine phosphatase SHP-1: potential role in proliferation and apoptosis. Cancer prevention research *4*, 1084-1094.

44. Shah, M., Patel, K., Mukhopadhyay, S., Xu, F., Guo, G., and Sehgal, P.B. (2006). Membrane-associated STAT3 and PY-STAT3 in the cytoplasm. J Biol Chem *281*, 7302-7308.

45. Tessem JS, Moss LG, Chao LC, Arlotto M, Lu D, Jensen MV, Stephens SB, Tontonoz P, Hohmeier HE, Newgard CB. Nkx6.1 regulates islet β-cell proliferation via Nr4a1 and Nr4a3 nuclear receptors. Proc Natl Acad Sci U S A. 2014 Apr 8;111(14):5242-7.

46. Hayes HL, Moss LG, Schisler JC, Haldeman JM, Zhang Z, Rosenberg PB, Newgard CB, Hohmeier HE. Pdx-1 activates islet α- and β-cell proliferation via a mechanism regulated by transient receptor potential cation channels 3 and 6 and extracellular signal-regulated kinases 1 and 2. Mol Cell Biol. 2013 Oct;33(20):4017-29.

47. Hucl T, Kylanpää-Bäck ML, Witt H, Künzli B, Lempinen M, Schneider A, Kemppainen E, Löhr M, Friess H, Ockenga J, Rosendahl J, Schulz HU, Gress T, Singer MV, Pfützer RH. HFE genotypes in patients with chronic pancreatitis and pancreatic adenocarcinoma. Genet Med. 2007 Jul;9(7):479-83.

48. Lu JP, Hayashi K, Awai M. Transferrin receptor expression in normal, iron-deficient and iron-overloaded rats. Acta Pathol Jpn. 1989 Dec;39(12):759-64.

49. Fuchs E, Horsley V. More than one way to skin. Genes Dev. 2008 Apr 15;22(8):976-85.

50. Fuchs E. Skin stem cells: rising to the surface. J Cell Biol. 2008 Jan 28;180(2):273-84.

51. Blanpain C, Fuchs E. Epidermal stem cells of the skin. Annu Rev Cell Dev Biol. 2006;22:339-73.

52. Tani H, Morris RJ, Kaur P. Enrichment for murine keratinocyte stem cells based on cell surface phenotype. Proc Natl Acad Sci U S A. 2000 Sep 26;97(20):10960-5.

53. Webb A, Li A, Kaur P. Location and phenotype of human adult keratinocyte stem cells of the skin. Differentiation. 2004 Oct;72(8):387-95.

54. Adams BD, Lazova R, Andrews NC, Milstone LM. Iron in skin of mice with three etiologies of systemic iron overload. J Invest Dermatol. 2005 Dec;125(6):1200-5.

55. Milstone LM, Hu RH, Dziura JD, Zhou J. Impact of epidermal desquamation on tissue stores of iron. J Dermatol Sci. 2012 Jul;67(1):9-14.

56. Milstone LM, Adams BD, Zhou J, Bruegel Sanchez VL, Shofner J. Stratum-specific expression of human transferrin receptor increases iron in mouse epidermis. J Invest Dermatol. 2006 Mar;126(3):648-52.

57. Coulombe PA, Kopan R, Fuchs E. Expression of keratin K14 in the epidermis and hair follicle: insights into complex programs of differentiation. J Cell Biol. 1989 Nov;109(5):2295-312.

58. Dassule HR, Lewis P, Bei M, Maas R, McMahon AP. Sonic hedgehog regulates growth and morphogenesis of the tooth. Development. 2000 Nov;127(22):4775-85.

59. Gritli-Linde A, Hallberg K, Harfe BD, Reyahi A, Kannius-Janson M, Nilsson J, Cobourne MT, Sharpe PT, McMahon AP, Linde A. Abnormal hair development and apparent follicular transformation to mammary gland in the absence of hedgehog signaling. Dev Cell. 2007 Jan;12(1):99-112.

60. Mazzalupo S, Wong P, Martin P, Coulombe PA. Role for keratins 6 and 17 during wound closure in embryonic mouse skin. Dev Dyn. 2003 Feb;226(2):356-65.

61. Chase HB, Montagna W, Malone JD. Changes in the skin in relation to the hair growth cycle. Anat Rec. 1953;116(1):75–81

62. Lo Celso C, Prowse DM, Watt FM. Transient activation of beta-catenin signalling in adult mouse epidermis is sufficient to induce new hair follicles but continuous activation is required to maintain hair follicle tumours. Development. 2004 Apr;131(8):1787-99.

63. Donati G, Proserpio V, Lichtenberger BM, Natsuga K, Sinclair R, Fujiwara H, Watt FM. Epidermal Wnt/β-catenin signaling regulates adipocyte differentiation via secretion of adipogenic factors. Proc Natl Acad Sci U S A. 2014 Apr 15;111(15):E1501-9.

Biography

I was born in Shanghai, China on August 6, 1980. I graduated from NC State University with a B.S. in Zoology in 2002 and a Masters of Genetics in 2004. I am published on the following papers:

Zhao C, Chen A, Jamieson CH, Fereshteh M, Abrahamsson A, Blum J, Kwon HY, Kim J, Chute JP, Rizzieri D, Munchhof M, VanArsdale T, Beachy PA, Reya T. Hedgehog signalling is essential for maintenance of cancer stem cells in myeloid leukaemia. Nature. 2009 Apr 9;458(7239):776-9.

Zhao C, Blum J, Chen A, Kwon HY, Jung SH, Cook JM, Lagoo A, Reya T. Loss of beta-catenin impairs the renewal of normal and CML stem cells in vivo. Cancer Cell. 2007 Dec;12(6):528-41.